

Deletion of Stim1 in hypothalamic arcuate nucleus Kiss1 neurons potentiates synchronous GCaMP activity and protects against diet-induced obesity

Jian Qiu^a, Todd L. Stincic^a, Martha A. Bosch^a, Ashley M. Connors^a, Stefanie Kaech Petrie ^b, Oline K. Rønneklev^{a,c}, Martin J. Kelly^{a,c}

Abbreviated title: Deletion of Stim1 of arcuate Kiss1 neurons potentiates the synchronous GCampP6 activity

^aDepartment of Chemical Physiology and Biochemistry, Oregon Health and Science University, Portland, United States

^bJungers Center for Neurosciences Research, Oregon Health and Science University, Portland, United States

^cDivision of Neuroscience, Oregon National Primate Research Center, Oregon Health and Science University, Beaverton, United States

Co-corresponding Authors:

Jian Qiu, Ph.D. and Martin J. Kelly, Ph.D.

Department of Chemical Physiology and Biochemistry

Oregon Health and Science University

3181 SW Sam Jackson Park Road

Portland, Oregon, 97239, United States

Tel: 503-494-5835

E-mail: giuj@ohsu.edu or kellym@ohsu.edu

Number of Pages:

Number of Figures: 7, Tables: 1, multimedia: 2,

Number of words for abstract: 250, introduction: 650, and discussion: 1500.

Conflict of interest statement: The authors declare that no competing interests exist.

Acknowledgements: This research was funded by National Institute of Health (NIH) grants: R01-NS043330 (OKR), R01-NS038809 (MJK) and R01-DK068098 (OKR and MJK). Confocal microscopy was supported by a P30 NS061800 (PI, S Aicher) grant. We thank Mr. Daniel Johnson for his technical support.

1 Abstract

2 Kisspeptin (Kiss1) neurons are essential for reproduction, but their role in the control of energy balance and other
3 homeostatic functions remains unclear. High frequency firing of hypothalamic arcuate Kiss1 ($\text{Kiss1}^{\text{ARH}}$) neurons
4 releases kisspeptin into the median eminence, and neurokinin B (NKB) and dynorphin onto neighboring $\text{Kiss1}^{\text{ARH}}$
5 neurons to generate a slow excitatory postsynaptic potential (EPSP) mediated by TRPC5 channels that entrains
6 intermittent, synchronous firing of $\text{Kiss1}^{\text{ARH}}$ neurons. High frequency optogenetic stimulation of $\text{Kiss1}^{\text{ARH}}$ neurons
7 releases glutamate to excite the anorexigenic proopiomelanocortin (POMC) neurons and inhibit the orexigenic
8 neuropeptide Y/agouti-related peptide (AgRP) neurons via metabotropic glutamate receptors. At the molecular
9 level, the endoplasmic reticulum calcium-sensing protein stromal interaction molecule 1 (STIM1) is critically
10 involved in the regulation of neuronal Ca^{2+} signaling and neuronal excitability through its interaction with plasma
11 membrane calcium (e.g., TRPC) channels. 17β -estradiol (E2) downregulates *Stim1* mRNA expression in female
12 arcuate neurons. Therefore, we hypothesized that deletion of *Stim1* in $\text{Kiss1}^{\text{ARH}}$ neurons would increase neuronal
13 excitability and their synchronous firing, which ultimately would affect energy homeostasis. Using optogenetics
14 in combination with whole-cell recording and GCaMP6 imaging in slices, we discovered that the deletion of *Stim1*
15 in Kiss1 neurons significantly increased the amplitude of the slow EPSP and augmented synchronous $[\text{Ca}^{2+}]_i$
16 oscillations in $\text{Kiss1}^{\text{ARH}}$ neurons. Deletion of *Stim1* in $\text{Kiss1}^{\text{ARH}}$ neurons amplified the actions of NKB and
17 protected ovariectomized female mice from developing obesity and glucose intolerance with high-fat dieting.
18 Therefore, STIM1 appears to play a critical role in regulating synchronous firing of $\text{Kiss1}^{\text{ARH}}$ neurons, which
19 ultimately affects energy homeostasis.

20 Significance Statement

21 Hypothalamic arcuate kisspeptin ($\text{Kiss1}^{\text{ARH}}$) neurons are essential for stimulating the pulsatile release of
22 gonadotropin releasing hormone (GnRH) and maintaining fertility. However, $\text{Kiss1}^{\text{ARH}}$ neurons appear to be a
23 key player in coordinating energy balance with reproduction. The regulation of calcium channels and hence
24 calcium signaling is critically dependent on the endoplasmic reticulum calcium-sensing protein stromal
25 interaction molecule 1 (STIM1), which interacts with the plasma membrane calcium channels. We have
26 conditionally deleted *Stim1* in $\text{Kiss1}^{\text{ARH}}$ neurons and found that it significantly increased the excitability of

27 Kiss1^{ARH} neurons and protected ovariectomized female mice from developing obesity and glucose intolerance
28 with high-fat dieting.

29

30

31 **Introduction**

32 Nutrition and reproduction are inextricably linked across all mammalian species, *i.e.*, high circulating
33 concentrations of 17 β -estradiol (E2) during the late follicular phase of the reproductive cycle correlate with
34 reduced food intake (Czaja, 1978; Asarian and Geary, 2006; Roepke et al., 2010). However, we are just
35 beginning to understand the central mechanisms by which E2 feedback coordinates reproduction and energy
36 balance (Castellano and Tena-Sempere, 2013; Nestor et al., 2014; Navarro, 2020). Kisspeptin neurons in the
37 hypothalamic arcuate nucleus (Kiss1^{ARH} neurons) appear to be critical for coordinating these two homeostatic
38 processes. Firstly, Kiss1 and its G protein-coupled receptor (GPR54) are essential for pubertal development
39 and reproductive function (Kuohung and Kaiser, 2006). Mutations in Kiss1 or GPR54 cause hypogonadotropic
40 hypogonadism in humans (De Roux et al., 2003; Seminara et al., 2003; Topaloglu et al., 2012), and deletion of
41 Kiss1 or GPR54 causes defective sexual development and reproductive failure in mice (Seminara et al., 2003;
42 d'Anglemont de Tassigny et al., 2007). These effects on fertility are directly dependent on Kiss1/GPR54 signaling
43 in gonadotropin-releasing hormone (GnRH) neurons (Han et al., 2005; Pielecka-Fortuna et al., 2008; Zhang et
44 al., 2008). Moreover, Kiss1 signaling appears to be also important for normal metabolism and glucose
45 homeostasis. GPR54 deletion in female, but not male, mice causes severe obesity, reduced metabolism, glucose
46 intolerance and hyperleptinemia (Tolson et al., 2014; Tolson et al., 2019). Also, Kiss1^{ARH} neurons are directly
47 depolarized/excited by leptin (Qiu et al., 2011) and insulin (Qiu et al., 2014), so they are quite possibly the key
48 neurons involved in conveying metabolic information to GnRH neurons.

49

50 High frequency optogenetic stimulation of Kiss1^{ARH} neurons expressing channel rhodopsin (ChR2) generates
51 pulsatile release of LH (Clarkson et al., 2017). Kiss1^{ARH} neurons co-express neurokinin B (NKB) and dynorphin
52 (Goodman et al., 2007; Navarro et al., 2009) and high-frequency firing (10-20 Hz) of these neurons co-releases
53 NKB and dynorphin to coordinate the synchronous firing of the whole population of Kiss1^{ARH} neurons (Qiu et al.,

54 2016). NKB binds to tachykinin 3 receptor (TacR3) in neighboring Kiss1^{ARH} neurons to activate canonical
55 transient receptor potential 5 (TRPC5) channels to cause a robust depolarization (slow EPSP), whereas co-
56 released dynorphin feeds back to bind to presynaptic κ-opioid receptors to limit the release of NKB to discrete
57 bursts of activity (Qiu et al., 2016). The co-release of the two peptide neurotransmitters coordinates the
58 synchronous firing of Kiss1^{ARH} neurons that drives the pulsatile release of GnRH into the median eminence (Qiu
59 et al., 2016; Clarkson et al., 2017).

60

61 The activity of TRPC channels is modulated by stromal-interaction molecule 1 (STIM1), which is localized
62 to the endoplasmic reticulum (ER) membrane of cells, and its N-terminal domain contains an EF-hand that
63 senses changes in ER calcium concentrations and maintains intracellular Ca²⁺ homeostasis through store-
64 operated Ca²⁺ entry (SOCE) (Salido et al., 2011). Upon depletion of ER Ca²⁺, STIM1 oligomerizes and then
65 interacts with plasma membrane calcium (TRPC) channels (Yuan et al., 2007; Salido et al., 2011).
66 Phosphorylation of STIM1 is required for oligomerization, and E2 inhibits the phosphorylation of STIM1 and its
67 interaction with plasma membrane Orai and TRPC channels and hence store-operated Ca²⁺ entry (Yuan et al.,
68 2007; Salido et al., 2011). Under normal physiological conditions, TRPC5 channels are coupled to plasma
69 membrane receptors (Qiu et al., 2010; Qiu et al., 2014; Gao et al., 2017), but in cellular stressed states (e.g.,
70 inflammation, obesity) TRPC5 channels may associate with STIM1 to replete ER Ca²⁺ stores (Birnbaumer, 2009;
71 Qiu et al., 2018b). E2 maintains the excitatory effects of insulin in POMC neurons, mediated by TRPC5 channel
72 opening, by downregulating *Stim1* expression, thereby protecting against insulin resistance in obese females
73 (Qiu et al., 2018b). E2 also downregulates *Stim1* expression in the ARH of female guinea pigs, indicating that
74 this interaction is more widespread in the ARH. Therefore, we hypothesized that deletion of *Stim1* in Kiss1^{ARH}
75 neurons would augment TacR3 mediated depolarization via TRPC5 channels to ultimately drive synchronous
76 firing of the “pulse generator Kiss1^{ARH} neurons.

77

78 **Materials and Methods**

79

80 *Animals*

81

82 All animal procedures were conducted at Oregon Health and Science University (OHSU) according to the
83 National Institutes of Health Guide for the Care and Use of Laboratory Animals and with approval from the OHSU
84 Animal Care and Use Committee.

85

86 We used female mice in all of the experiments. *Kiss1*^{Cre:GFP} (v2) mice (Dr. Richard D. Palmiter; University of
87 Washington; PMID: 29336844) (Padilla et al., 2018) were housed under constant temperature (21–23°C) and
88 12-h light, 12-h dark cycle schedule (lights on at 0600 and lights off at 1800 h), with free access to food (Lab
89 Diets 5L0D) and water. *Kiss1*^{Cre:GFP} mice were used for viral injection to express ChR2 or GCaMP6s in *Kiss1*^{ARH}
90 neurons or they were crossed with heterozygous *Ai32* mice (RRID:IMSR_JAX:024109, C57BL/6 background)
91 purchased from The Jackson Laboratory. These *Ai32* mice carry the ChR2 (H134R)–EYFP gene in their
92 Gt(ROSA)26Sor locus (Madisen et al., 2012). The gene is separated from its CAG promoter by a loxP-flanked
93 transcriptional STOP cassette, allowing its expression in a Cre-dependent manner. To test for this we dispersed
94 and harvested EYFP neurons in the ARH from *Kiss1*^{Cre:GFP};*:Ai32* females and used single cell RT-PCR to
95 determine *Kiss1* mRNA expression as described below and according to previous published methods (Bosch et
96 al., 2013). Data from 126 ARH^{EYFP} neurons from 6 *Kiss1*^{Cre:GFP};*:Ai32* females documented that 99% of the EYFP
97 neurons expressed *Kiss1*.

98

99 To generate mice with conditional knockout of *Stim1* in *Kiss1* neurons (*Stim1*^{KKO}), we first crossed *Kiss1*^{Cre/+}
100 (v2) males (Padilla et al., 2018) with *Stim1*^{loxP/loxP} females (Jackson Laboratory Stock #023350,
101 RRID:IMSR_JAX:023350, (Oh-hora et al., 2008)). This cross knocks out *Stim1* through excising exon 2 (Oh-
102 hora et al., 2008) of the floxed *Stim1* gene in cells in which Cre is expressed under the control of a promoter
103 specific for the expression of *Kiss1* (Padilla et al., 2018; Qiu et al., 2018a). The F1 mice produced were
104 *Kiss1*^{Cre/+};*:Stim1*^{+/lox} and *Stim1*^{+/lox}. The F2 mice were generated by crossing these *Kiss1*^{Cre/+};*:Stim1*^{+/lox} males
105 with *Stim1*^{loxP/lox} females. Approximately 25% of the offspring were *Kiss1*^{Cre/+};*:Stim1*^{lox/lox} such that *Stim1* was
106 deleted in *Kiss1* cells (*Stim1*^{KKO}), and all the *Stim1* knock-out mice were seen at the expected frequency and
107 viable throughout adulthood. We used *Kiss1*^{Cre/+} mice as controls. To increase the yield of *Stim1* knock-out mice,

108 we crossed $\text{Kiss1}^{\text{Cre/+}}\text{::Stim1}^{\text{lox/lox}}$ males with $\text{Stim1}^{\text{lox/lox}}$ females. We maintained not only this strain but also the
109 $\text{Kiss1}^{\text{Cre/+}}$ strain at the same time. Genotypes for *Stim1* were determined using forward primer JAX#18885 (5'-
110 CGA TGG TCT CAC GGT CTC TA-3') and reverse primer JAX#18886 (5'-GCT CTG CTG ACC TGG AAC TA-
111 3'), which distinguished between lox/lox, lox/+, and +/+ genotypes. Cre genotypes were determined using
112 forward primer 5'-GCG GTC TGG CAG TAA AAA CTA TC3'- and reverse primer 5'-TTC CAT GAG TGA ACG
113 AAC CTG G-3', which distinguished between carriers and non-carriers of the Cre allele.

114
115
116 *Puberty onset and estrous cyclicity*

117 To determine whether deleting *Stim1* in *Kiss1*-expressing neurons might impact fertility, we evaluated female
118 Stim1^{kko} mice and wild type (WT) female littermates for pubertal onset and estrous cyclicity. For breeding, male
119 and female mice were mated at 1:1, and the number of pups per litter was counted. The Stim1^{kko} mice showed
120 similar fecundity as control mice. Puberty onset in females was assessed by monitoring for vaginal opening daily
121 between 0900 and 1000 hr starting at 3 weeks of age. For estrous cycle studies, Stim1^{kko} and $\text{Kiss1}^{\text{Cre:GFP}}$ female
122 mice were group housed and were habituated to handling for at least one week by the same investigator prior to
123 estrous cycle monitoring. Vaginal lavage was performed daily for 13 consecutive days between 0900 and 1000
124 hr. Cytology was evaluated using a light microscope and scored as diestrus, proestrus or estrus as previously
125 described (Qiu et al., 2018a). The Number of estrous and diestrous days were counted for each animal and used
126 for statistical analysis (Mann-Whitney U-test).

127
128 *Gonadectomy*

129 At least 7 days prior to each experiment, ovaries were removed as described previously while under inhalant
130 isofluorane anesthesia (Piramal Enterprises Limited, Andhra Pradesh, India) (Qiu et al., 2018a). Each mouse
131 received analgesia (Carprofen; 5mg/kg; subcutaneous) immediately after a surgery for relief of postoperative
132 pain.

133
134 *Metabolic Studies*

135 For the metabolic studies, *Stim1^{kk0}* and *Kiss1* littermate control females were ovariectomized at 2-4 months
136 of age and put on a high fat diet (HFD; 45% kcal from fat; Research Diets, New Brunswick, NJ; D12451) for eight
137 weeks. Mice were group housed (because of COVID-19 restrictions) and individually weighed every week. The
138 evening prior to the glucose tolerance test (GTT), all mice were assessed for body composition (fat and lean
139 mass) using an EchoMRI 4-in-1-500 Body Composition Analyzer (Houston, TX).

140

141 For GTT, age matched *Kiss1^{Cre}* and *Stim1^{kk0}* mice were fasted overnight for 15-h, and baseline glucose
142 levels measured with the aid of an Accu-Check Advantage blood glucose meter (Roche) using blood collected
143 from the tail vein. All mice were then injected intraperitoneally with glucose (1 mg/g lean mass as determined by
144 EchoMRI) in sterile PBS and blood glucose levels were measured 15, 30, 60, 90, and 120 min after injection.
145 The glucose clearance (area under the curve) was calculated based on the glucose baseline levels at 0 min
146 (Ayala et al., 2010).

147

148

149 AAV delivery to *Kiss1^{Cre:GFP}* and *Stim1^{kk0}* mice

150 Fourteen to twenty-one days prior to each experiment, *Kiss1^{Cre:GFP}* mice or *Stim1^{kk0}* mice (>60 days old)
151 received bilateral ARH injections of a Cre-dependent adeno-associated viral (AAV; serotype 1) vector encoding
152 ChR2-mCherry (AAV1-Ef1a-DIO-ChR2: mCherry) or ChR2-YFP (AAV1-Ef1a-DIO-ChR2:YFP, Dr. Stephanie L.
153 Padilla; University of Washington; PMID: 25429312) or GCaMP6s (AAV9-Syn-Flex-GCaMP6s-WPRE-SV40;
154 Addgene, # 100845-AAV9). Using aseptic techniques, anesthetized female mice (1.5% isoflurane/O₂) received
155 a medial skin incision to expose the surface of the skull. The glass pipette (Drummond Scientific #3-000-203-
156 G/X; Broomall, PA) with a beveled tip (diameter = 45 μ m) was filled with mineral oil, loaded with an aliquot of
157 AAV using a Nanoject II (Drummond Scientific). ARH injection coordinates were anteroposterior (AP): -1.20 mm,
158 mediolateral (ML): \pm 0.30 mm, dorsoventral (DL): -5.80 mm (surface of brain z = 0.0 mm); 500 nl of the AAV
159 (2.0 x 10¹² particles/ml) was injected (100 nl/min) into each position, left in place for 10 min post-injection, then
160 the pipette was slowly removed from the brain. The skin incision was closed using skin adhesive, and each
161 mouse received analgesia (Carprofen; 5 mg/kg) for two days post-operation.

162

163 *Electrophysiology*

164 Coronal brain slices (250 μ m) containing the ARH from gonadectomized females were prepared as
165 previously described (Qiu et al., 2003). Whole-cell, patch recordings were performed in voltage clamp and
166 current clamp using an Olympus BX51W1 upright microscope equipped with video-enhanced, infrared-
167 differential interference contrast (IR-DIC) and an Exfo X-Cite 120 Series fluorescence light source. Electrodes
168 were fabricated from borosilicate glass (1.5 mm outer diameter; World Precision Instruments, Sarasota, FL) and
169 filled with a normal internal solution (in mM): 128 potassium gluconate, 10 NaCl, 1 MgCl₂, 11 EGTA, 10 HEPES,
170 3 ATP, and 0.25 GTP (pH was adjusted to 7.3–7.4 with 1N KOH, 290–300 mOsm). Pipette resistances ranged
171 from 3–5 M Ω . In whole cell configuration, access resistance was less than 20 M Ω ; access resistance was 80%
172 compensated. For some experiments measuring the ramp current–voltage (I–V) relationship, K⁺-gluconate in the
173 normal internal solution was replaced with Cs⁺-gluconate (pH 7.35 with CsOH), and the extracellular solution
174 contained Na⁺, K⁺, I_h (HCN), Ca²⁺, and GABA_A channel blockers (in mM: NaCl, 126; 4-aminopyridine, 5; KCl, 2.5;
175 MgCl₂, 1.2; CsCl, 2; CaCl₂, 1.4; CoCl₂, 1; nifedipine, 0.01; HEPES, 20; NaOH, 8; glucose, 10; tetrodotoxin, 0.001;
176 picrotoxin, 0.1). For optogenetic stimulation, a light-induced response was evoked using a light-emitting diode
177 (LED) 470 nm blue light source controlled by a variable 2A driver (ThorLabs, Newton, NJ) with the light path
178 delivered directly through an Olympus 40 water-immersion lens. High fidelity response to light (470 nm)
179 stimulation of Kiss1^{ARH} ::ChR2-mCherry expressing neurons was observed, and both evoked inward currents (in
180 voltage clamp, V_{hold} = -60 mV) or depolarization (in current clamp) were measured. Electrophysiological signals
181 were amplified with an Axopatch 200A and digitized with Digidata 1322A (Molecular Devices, Foster City, CA),
182 and the data were analyzed using p-Clamp software (RRID:SCR_011323, version 9.2, Molecular Devices). The
183 amplitude of the slow EPSP was measured after low pass filtering in order to eliminate the barrage of action
184 potentials riding on the depolarization. The liquid junction potential was corrected for all data analysis.

185

186 *Calcium imaging*

187 For calcium imaging, brain slices were placed in a RC-22C slide recording chamber (Harvard/Warner
188 Instruments) and imaged on an inverted Nikon TiE microscope equipped with a Yokogawa CSU-W1 spinning

189 disk confocal head, integrated under NIS Elements v4.20 (Nikon). The preparation, kept at 32°C via a cage
190 incubator (Okolab), was continuously perfused with oxygenated aCSF at a flow rate of 1.25 ml/min. Images were
191 acquired on a Zyla v5.5 sCMOS camera (Andor) at 0.5 Hz. frame-rate, through an 10 x (NA 0.45) or 20 x (NA
192 0.75) objective, combining 488 nm laser excitation with 500–550 nm emission collection. A single focal plane (z-
193 axis) was maintained using the Nikon Perfect Focus System. Minor tissue drift in the x-y axis was corrected
194 using NIS Elements. Imaging displaying major drift were excluded from final analysis. Changes in Kiss1^{ARH}
195 neuron Ca²⁺ levels were measured in regions of interest (ROIs) comprising the GCaMP6s-positive cell bodies.
196 In all recordings, background fluorescence measured in an ROI drawn on nearby tissue was subtracted from
197 every ROI. [Ca²⁺] variations after drug applications were assessed as changes in fluorescence signals over
198 baseline ($\Delta F/F_0$). To normalize the fluorescence value of each cell, we first separated experimental trials into
199 two parts: a baseline period (2 min) corresponding to all the frames recorded before addition of drugs, and a
200 stimulus period, after the onset of the drug (such as bath-applied senktide) application and lasting several
201 minutes. Next, for each ROI we calculated $\Delta F/F_0$ for each frame (t), where $\Delta F/F_0$ equals $(F_{(t)} - F_0)/F_0$, and F_0 was
202 the mean fluorescence value for that ROI for all frames in the baseline period for that trial. The area under the
203 curve (AUC) was calculated over the time periods of 2 min before and 18 min after drug application. Maximal
204 peak reached after drug application was also measured and used in quantitative analysis. Data were averaged
205 across all Kiss1^{ARH} neurons in a slice (two slices per animal), which were used as the statistical unit over a
206 minimum of 3 animals per condition.

207
208 *Single cell RT-PCR (scRT-PCR)*
209 Coronal brain sections from the ARH of three female *Stim1*^{kk0} and three *Kiss1*^{Cre:GFP}::*Ai32* mice were prepared
210 for electrophysiology and scRT-PCR. The 3-4 slices obtained were divided between electrophysiological
211 recording experiments and single cell harvesting. Single cell dispersion and harvesting was performed as
212 described previously with some modifications as described below (Bosch et al., 2013; Zhang et al., 2013b).
213 Briefly, the ARH was dissected and digested in papain (7mg/ml in aCSF, Sigma-Aldrich). Gentle trituration using
214 varying sizes of flame polished Pasteur pipets were used to disperse the cells and then they were plated onto a
215 glass bottom dish. A constant flow of oxygenated aCSF (NaCl, 125 mM; KCl, 5 mM; NaH₂PO₄, 1.44 mM; Hepes,

216 5 mM; D-glucose, 10 mM; NaHCO₃, 26 mM; MgSO₄·7H₂O, 2 mM; CaCl₂, 2 mM) was applied to the dish to keep
217 the cells healthy and to clear debris. Fluorescent neurons were visualized under an inverted microscope. The
218 Xenoworks Microinjection system (Sutter Instruments) was used to manipulate a 10 µm tip size glass capillary
219 tube to approach single neurons, apply gently suction and harvest single cells or pools of 10 cells into a
220 siliconized tube containing a solution of 1X Invitrogen Superscript III Buffer (LifeTech), 15U of RNasin (Promega),
221 10 mM of dithiothreitol (DTT) and diethylpyrocarbonate (DEPC)-treated water in a total of 5 µl for single cells or
222 8 µl for pools of 10 cells. Corresponding controls were collected at the same time including single neurons
223 (processed without reverse transcriptase) and aCSF from the surrounding area. Hypothalamic tissue RNA was
224 also processed with and without reverse transcriptase. First strand cDNA synthesis was performed on single
225 cells, pools of cells and controls in a 20 µl (single cells) or 25 µl (10 cell pools) volume containing a final
226 concentration of 1X Invitrogen Superscript III Buffer, 30 U of RNasin, 15 mM DTT, 10 mM dNTP, 100 ng Random
227 Primers (Promega), 400 ng Anchored Oligo (dT)₂₀ Primer (Invitrogen), 100 U Superscript III Reverse
228 Transcriptase (Life Tech) and DEPC-treated water according to manufactures protocol and stored at -20°C.
229 Clone Manager software (Sci Ed Software) was used to design primers that cross at least one intron-exon
230 boundary. In order to confirm that STIM1 was knocked out, STIM1 primers were designed to include part of
231 exon 2 (see Table 1). Single cell PCR conditions were optimized for primer concentration, magnesium
232 concentration and annealing temperature. Standard curves were generated using hypothalamic cDNA with
233 dilutions from 1:50 to 1:12,800 for primers used for qPCR to determine the efficiency ($E = 10^{(-1/m)} - 1$; table 1).
234 Primer pairs with efficiencies of 90-100% permit the use of the comparative $\Delta\Delta CT$ method for analysis (Livak
235 and Schmittgen, 2001; Pfaffl, 2001).

236

237 PCR for *Kiss1*, *Stim1*, *Trpc4* and *Trpc5* mRNAs was performed on 3 µl of cDNA from single cells in a 30 µl
238 reaction volume containing 1X GoTaq Flexi buffer (Promega), 2 mM MgCl₂, 10 mM dNTP, 0.33 µM forward and
239 reverse primers, 2 U GoTaq Flexi Polymerase (Promega) and 0.22 µg TaqStart Antibody (Clontech). 45-50
240 cycles of amplification were performed on a Bio-Rad C1000 thermocycler and the resulting product visualized
241 with ethidium bromide on a 2% agarose gel.

242

243 Quantitative PCR (qPCR) was performed on 3-4 μ l of cDNA from pools of 5-10 cells (3-4 pools/animal) in
244 duplicate for the target genes (*Stim1*, *Stim2*, *Trpc4* and *Trpc5*) and 2 μ l in duplicate for the reference gene
245 (*Gapdh*) in a 20 μ l reaction volume containing 1X Power SYBR Green PCR Master Mix (Applied Biosystems)
246 and 0.5 μ M forward and reverse primers. Forty cycles of amplification were run on a Quant Studio 7 Flex Real-
247 Time PCR System (Applied Biosystems) and the resulting data was analyzed using the comparative $\Delta\Delta CT$
248 method (Livak and Schmittgen, 2001; Pfaffl, 2001). The relative linear quantity was determined with the $2^{-\Delta\Delta CT}$
249 equation (Bosch et al., 2013). The mean of all of the ΔCT values ($\Delta CT = CT$ of the target gene – CT of the
250 reference gene) from the controls was used as the calibrator and the data is expressed as fold change in gene
251 expression.

252

253 *Drugs*

254 A standard artificial cerebrospinal fluid was used (Qiu et al., 2011). All drugs were purchased from Tocris
255 Bioscience (Minneapolis, MN) unless otherwise specified. Tetrodotoxin (TTX) was purchased from Alomone
256 Labs (Jerusalem, Israel) (1 mM) and dissolved in H₂O. Thapsigargin (Tg, 2 mM), TacR3 agonist senktide (1 mM)
257 and TRPC4/5 antagonist, HC 070 (from MedChemExpress, 10 mM) were prepared in dimethylsulfoxide (DMSO).
258 Aliquots of the stock solutions were stored as appropriate until needed.

259

260 *Data analysis*

261 For qPCR four Kiss1 neuronal pools (10 cells/pool) from each animal were run in duplicate for the mRNAs
262 that encode for STIM1, STIM2 and GAPDH and the mean value of each gene from each animal (n = 3 animals)
263 was used for statistical analysis. Data are expressed as mean \pm SEM and were analyzed using an unpaired
264 student's t-test. In addition, Kiss1 neuronal pools (5-10 cells/pool) were used to determine the expression of
265 *Trpc4* and *Trpc5* in these neurons. For scRT-PCR the number of Kiss1-positive cells harvested from Kiss1^{Cre:GFP}
266 females injected with Cre-dependent ChR2-mCherry or from Kiss1^{Cre:GFP::Ai32} females were used to qualitatively
267 assess the number of Kiss1 neurons with *Stim1*, *Stim2*, *Trpc4*, *Trpc5* and percent expression.

268

269 Comparisons between different treatments were performed using a repeated measures, two-way or one-way

270 ANOVA analysis with the *post hoc* Bonferroni's test. Differences were considered statistically significant if $p <$
271 0.05. All data are expressed as mean \pm SEM.

272

273

274 **Results**

275

276 *Validation of conditional deletion of Stim1 in Kiss1 neurons*

277 STIM1 is involved in the regulation of neuronal firing in cerebellar Purkinje neurons (Hartmann et al., 2014;
278 Ryu et al., 2017), dopaminergic neurons (Sun et al., 2017) and hypothalamic arcuate POMC neurons (Qiu et al.,
279 2018b). Initially to see if STIM1 regulates Kiss1^{ARH} neuronal excitability, we measured the mRNA expression of
280 *Stim1* and its close homolog *Stim2* in manually harvested Kiss1^{ARH} neurons by quantitative real-time PCR
281 (**Figure 1A**). Based on the qPCR, mRNA levels of *Stim1* were greater than those of *Stim2* in Kiss1^{ARH} neurons
282 (**Figure 1A1**). Likewise, in cerebellar Purkinje neurons, *Stim1* is also much more abundant than *Stim2* (Hartmann
283 et al., 2014), while in hippocampal (Berna-Erro et al., 2009) and cortical neurons (Gruszczynska-Biegala et al.,
284 2011) *Stim2* expression levels exceed those of *Stim1*. A qualitative, unbiased sampling of Kiss1^{ARH} neurons
285 (n=60) from ovariectomized *Kiss1^{Cre}* females (n =3) revealed that *Stim1* mRNA was expressed in 81.7 ± 7.6
286 percent and *Stim2* mRNA was detected in 81.2 ± 2.7 percent of Kiss1^{ARH} neurons with 70 percent of neurons
287 expressing both *Stim1* and *Stim2*.

288

289 To elucidate the functional role of STIM1 in Kiss1 neurons, we generated mice that lack STIM1 selectively in
290 Kiss1 neurons (*Stim1^{ko}*, detailed in Methods). We confirmed the *Stim1* deletion in *Stim1^{ko}* mice using single cell
291 quantitative PCR of pools of harvested Kiss1^{ARH} neurons (n= 3 animals) (**Figure 1A2**). Consistent with the scRT-
292 PCR results (**Figure 1B**), *Stim1* mRNA was undetectable in *Stim1^{ko}* neurons (**Figure 1A2**), whereas there was
293 no reduction in *Stim2* mRNA expression (**Figure 1A3**). In contrast, *Stim1* mRNA was still expressed in the
294 majority of adjacent nonfluorescent neurons obtained from both *Stim1^{ko}* and *Kiss1^{Cre}* mice.

295

296 *Stim1 deletion reduces Store Operated Calcium Entry (SOCE)*

297 SOCE constitutes an important source of calcium entry and signaling in neurons. Depletion of ER Ca^{2+} stores
298 causes the ER Ca^{2+} sensor STIM proteins (STIM1 and STIM2) to interact with and activate cell surface Ca^{2+}
299 release-activated Ca^{2+} (CRAC) channels, thereby resulting in a second wave of cytoplasmic Ca^{2+} rise (Moccia
300 et al., 2015). Genetic suppression of *Stim1* in neural progenitor cells results in abrogation of this second wave
301 of calcium rise that constitutes SOCE (Somasundaram et al., 2014). We asked whether deletion of *Stim1* in
302 $\text{Kiss1}^{\text{ARH}}$ neurons (*Stim1*^{kk0}) attenuates neuronal SOCE. $\text{Kiss1}^{\text{Cre}}$ and *Stim1*^{kk0} mice received bilateral ARH
303 injections of GCaMP6 viral vector (**Figure 1C1, C2**), and the $\text{Kiss1}^{\text{ARH}}$ or *Stim1*^{kk0} neurons with GCaMP6s in
304 slices were imaged using spinning disk confocal microscopy (**Figure 2-video supplement 1**). ER Ca^{2+} stores
305 were released by treatment with 2 μM thapsigargin (Tg), a blocker of the SERCA (sarcoplasmic/endoplasmic
306 reticulum Ca^{2+} ATPase) pump. As expected, Tg treatment of neurons bathed in Ca^{2+} -free aCSF generated an
307 initial wave of cytoplasmic Ca^{2+} release ($[\text{Ca}^{2+}]_i$) as measured by an increase in GCaMP6s activity both in control
308 and *Stim1*-deleted neurons (**Figure 1D, E and F**). As long as neurons were kept in Ca^{2+} - free aCSF, the ER
309 stores remained empty, a situation that was presumably sensed by the Ca^{2+} sensor STIMs. Upon switching to a
310 normal aCSF containing 2 mM Ca^{2+} , an immediate SOCE response was observed as a second wave of
311 cytoplasmic Ca^{2+} rise. Consistent with a role for STIM1 regulation, we observed an attenuation of SOCE in
312 *Stim1*^{kk0} neurons (**Figure 1D, E, F and G**: $\Delta F/F_0 * 100 = 1274.5 \pm 49.4$, $n = 4$, $\text{Kiss1}^{\text{ARH}}$ group versus 389.0 ± 86.1 ,
313 $n = 4$, *Stim1*^{kk0} group, which was measured from the 15 minute time point to the peak, unpaired t-test, $t_{(6)} = 8.921$,
314 $p = 0.0001$, *** $p < 0.005$), indicating that STIM1 plays a major role in SOCE after Tg-induced ER Ca^{2+} depletion
315 in $\text{Kiss1}^{\text{ARH}}$ neurons as has been shown in other CNS neurons (Guner et al., 2017; Pavez et al., 2019).

316
317 *TacR3* -induced increase in $[\text{Ca}^{2+}]_i$ is augmented by deletion of *Stim1*

318 *TacR3* classically couples to a G α q protein-calcium signaling and excites $\text{Kiss1}^{\text{ARH}}$ neurons (de Croft et al.,
319 2013; Ruka et al., 2013; Qiu et al., 2016). Calcium is of critical importance to neurons as it participates in the
320 transmission of depolarizing signals and contributes to synaptic activity (Brini et al., 2014). Therefore, we tested
321 whether STIM1 can modulate *TacR3*-mediated calcium responses. We first measured the effects of the *TacR3*,
322 which is G α q-coupled, agonist senktide on GCaMP6s-expressing $\text{Kiss1}^{\text{ARH}}$ neurons in arcuate slices from $\text{Kiss1}^{\text{Cre}}$
323 mice; senktide (1 μM) rapidly induced an increase in $[\text{Ca}^{2+}]_i$ (**Figures 2A,C**). Next, we investigated if STIM1

324 contributes to intracellular rise in $[Ca^{2+}]_i$ after senktide activation. Indeed, deletion of *Stim1* significantly
325 augmented the peak TacR3-mediated response by ~three-fold ($\Delta F/F_0 \times 100 = 244.0 \pm 27.7$, n = 7 slices, $Kiss1^{ARH}$
326 group versus 622.1 ± 133.2 , n = 6 slices), *Stim1^{kk0}* group; two-way ANOVA: main effect of treatment ($F_{(1,11)} =$
327 5.265 , $p = 0.0424$), main effect of time ($F_{(19,209)} = 42.69$, $p < 0.0001$) and interaction ($F_{(19,209)} = 6.486$, $p < 0.0001$);
328 *post hoc* Bonferroni test, **** $p < 0.001$; ** $p < 0.01$; * $p < 0.05$). (**Figures 2B, C**). Likewise, the area under the
329 curve was significantly increased in the *Stim1^{kk0}* group by four-fold ($Kiss1^{cre}$: 954.8 ± 200.4 , n = 7 versus $Kiss1^{kk0}$:
330 3746.0 ± 1227.0 , n = 6) (**Figure 2D**).

331 *Deletion of STIM1 enhances slow EPSP in Kiss1^{ARH} neurons*

332 Kiss1^{ARH} neurons are the chief component of the GnRH pulse generator circuit (Navarro et al., 2009; Lehman
333 et al., 2010; Navarro et al., 2011; Okamura et al., 2013), such that they synchronize their activity to trigger the
334 release of peptides to drive pulsatile release of GnRH (Qiu et al., 2016; Clarkson et al., 2017). To investigate if
335 STIM1 modulates the activity of Kiss1^{ARH} neurons, we bilaterally injected AAV1-Ef1a-DIO-ChR2:mCherry into
336 the arcuate nucleus of *Kiss1^{Cre}* and *Stim1^{kk0}* mice. To verify that *Trpc5* mRNAs is co-localized in these Kiss1^{ARH}
337 neurons, we harvested 50 Kiss1^{ARH} neurons from 2 females and did scRT-PCR for *Trpc5* and *Trpc4* expression.
338 The single-cell analysis revealed that *Trpc5* transcript was detectable in 82% of Kiss1^{ARH} neurons, but *Trpc4*
339 mRNA was not detected in Kiss1^{ARH} neurons (**Figure 3A**). Moreover, quantitative single cell PCR documented
340 that *Trpc5* but not *Trpc4* mRNA was expressed in Kiss1^{ARH} neurons (**Figure 3B**). With whole-cell recording we
341 verified the expression of TRPC5 channels by documenting the senktide - induced typical double-rectifying I/V
342 plot characteristic of the activation of TRPC5 channels (**Figure 3C**) as we previously reported (Kelly et al., 2018).
343 Initially, whole-cell patch recording in *Kiss1^{ARH}* neurons from ovariectomized *Kiss1* or *Stim1^{kk0}* female mice
344 revealed that there was no difference in the resting membrane potential (RMP: *Kiss1*: -66.0 ± 1.7 mV, n = 38
345 versus *Stim1^{kk0}*: -68.2 ± 0.9 mV, n = 58) or membrane capacitance (C_m : *Kiss1*: 25.0 ± 1.0 pF, n = 38 versus
346 *Stim1^{kk0}*: 27.3 ± 0.9 pF, n = 58). However, there was a significant difference in the membrane input resistance
347 (R_{in} : *Kiss1*: 524.2 ± 42.4 Ω , n = 38, versus *Stim1^{kk0}*: 417.3 ± 26.9 Ω , n = 58, unpaired two-tailed *t* test, $t_{(94)} =$
348 2.242 , $p = 0.0273$), which has also been reported with *Stim1* knockout in cerebellar Purkinje neurons (Ryu et
349 al., 2017). Kiss1^{ARH} neurons expressing ChR2-mCherry in slices were photostimulated at 20 Hz for 10 s (**Figure**

350 **3-video supplement 1)** to generate slow EPSPs as previously described (Qiu et al., 2016). As we had
351 hypothesized, deletion of *Stim1* augmented the slow EPSP induced by high-frequency optogenetic stimulation
352 (**Figure 3D-F**). Also in the presence of TTX to block voltage-gated Na⁺ channels, we observed that senktide
353 induced larger inward currents in Kiss1^{ARH} neurons from *Stim1^{kk0}* mice versus *Kiss1^{Cre}* mice (**Figure 4A-C**).
354 Although the senktide-induced cation current was significantly increased by *Stim1* deletion, the I/V plots revealed
355 that the reversal potential for the current was not different between Kiss1^{ARH} neurons recorded from *Stim1^{kk0}*
356 mice or *Kiss1^{Cre}* mice (*Kiss1*: -10.5 ± 2.1 mV, n = 4, vs *Stim1^{kk0}*: -9.8 ± 2.2 mV, n = 4, unpaired two-tailed t test,
357 t₍₆₎ = 0.2503, p = 0.8107) (**Figure 4D-F**). These results indicate that STIM1 expression governs the activity of
358 TRPC5 channels, which contribute to the synchronous activity of Kiss1^{ARH} neurons.

359
360 ***NKB agonist activates TRPC5 channels in Kiss1^{ARH} neurons from Kiss1^{Cre} and Stim1^{kk0} mice***
361 Based on our previous findings that TRPC5 channel protein is expressed in Kiss1^{ARH} neurons and is activated
362 by the NKB agonist senktide (Qiu et al., 2011; Kelly et al., 2018), we investigated the contribution of TRPC5
363 channels to generating the slow EPSP. We used a ratio method in which a slow EPSP was generated by
364 optogenetic stimulation (20 Hz, 10 s) of Kiss1^{Cre}:ChR2 neurons and then stimulated again 10 min later after drug
365 exposure (Qiu et al., 2016). For the Kiss1^{ARH} neurons from ovariectomized female *Kiss1:Ai32* mice, the RMP,
366 C_m and R_{in} were -72.7 ± 0.8 mV, 22.4 ± 0.7 pF and 458.6 ± 23.3 Ω, n = 50, respectively. Using this protocol, we
367 found that the slow EPSP was inhibited by perfusing the TRPC4/5 channel blocker HC 070 (100 nM) (Just et al.,
368 2018) for 5 minutes, and the ratio was significantly decreased from 60 to 30 percent (**Figure 5A-C**). Since *Trpc4*
369 mRNA is not expressed in Kiss1^{ARH} neurons (**Figure 3A, B**), we would argue that TRPC5 channels mediate the
370 slow EPSP in these neurons. To elucidate the TRPC5 channel contribution to the postsynaptic activity of
371 Kiss1^{ARH} neurons from *Stim1^{kk0}* mice, we perfused TTX to block fast sodium channels and found that HC 070
372 significantly suppressed the senktide-induced inward current (**Figure 5D, E and F**).

373
374 ***Stim1 deletion in Kiss1^{ARH} neurons has minimal effects on estrous cycle***
375 *Stim1^{kk0}* mice on the C57BL/6 background were viable at the expected Mendelian ratio and did not show
376 any difference in the time to vaginal opening (*Stim1^{kk0}* mice: postnatal day 30.2 ± 0.8, n = 21 versus *Kiss1^{Cre}*

377 mice: postnatal day 29.1 ± 0.8 , $n = 19$, Unpaired t test, $t_{(38)} = 1.003$, $p = 0.3222$). However, since kisspeptin
378 neurons are responsible for the maintenance of the reproductive cycle (Seminara et al., 2003; d'Anglemont de
379 Tassigny et al., 2007; Mayer et al., 2010), and *Stim1* deletion facilitated the synchronous firing of $\text{Kiss1}^{\text{ARH}}$
380 neurons, we measured the effects of *Stim1* deletion in Kiss1 neurons on the estrous cycle. We monitored the
381 estrous cycle of *Stim1*^{kk0} and $\text{Kiss1}^{\text{Cre}}$ female mice with vaginal lavage for two weeks before ovariectomy for the
382 metabolic studies (see below). *Stim1*^{kk0} female mice exhibited prolonged estrous cycles versus the $\text{Kiss1}^{\text{Cre}}$
383 females (**Figure 6A,B,C versus 6D,E,F**) with a slight prolongation of estrous days (**Figure 6H**). Although more
384 in depth analysis is warranted (i.e., measurement of pulsatile LH), the results were not unexpected since
385 augmented synchronous activity of $\text{Kiss1}^{\text{ARH}}$ neurons, as we documented at the cellular level, should still drive
386 luteinizing hormone (LH) pulses in these female mice (Qiu et al., 2016; Clarkson et al., 2017).

387

388 *Stim1* deletion in $\text{Kiss1}^{\text{ARH}}$ neurons protects ovariectomized females against diet-induced obesity

389 Subsequently, the same two cohorts of female mice, *Stim1*^{kk0} ($n=10$) and the littermate control $\text{Kiss1}^{\text{Cre}}$
390 ($n=10$) mice, were ovariectomized at around 3 months of age and put on a high fat diet for eight weeks (see
391 Methods). Over this time period, there was significantly less gain in body weight in the *Stim1*^{kk0} versus the
392 $\text{Kiss1}^{\text{Cre}}$ mice (**Figure 7A, B**). Moreover, the average fat mass of *Stim1*^{kk0} mice was significantly lighter than that
393 of $\text{Kiss1}^{\text{Cre}}$ controls by week 6 (*Stim1*^{kk0} versus $\text{Kiss1}^{\text{Cre}}$ mice fat mass: 7.6 ± 0.9 g, $n=10$ versus 11.4 ± 1.1 g,
394 $n=10$) (**Figure 7C**). The lean mass of *Stim1*^{kk0} mice was also significantly less versus the $\text{Kiss1}^{\text{Cre}}$ mice (*Stim1*^{kk0}
395 versus the $\text{Kiss1}^{\text{Cre}}$ mice lean mass: 16.9 ± 0.4 g, $n=10$ versus 18.9 ± 0.4 g, $n=10$) (**Figure 7D**). After 6 weeks,
396 both *Stim1*^{kk0} and $\text{Kiss1}^{\text{Cre}}$ controls were assessed for glucose tolerance using an *i.p.* glucose tolerance test (see
397 Methods). Both *Stim1*^{kk0} and $\text{Kiss1}^{\text{Cre}}$ females started at relatively the same blood glucose levels after an
398 overnight fast (**Figure 7E, time 0**), suggesting similar whole-body homeostatic conditions after fasting. However,
399 *Stim1*^{kk0} female mice had significantly lower glucose levels after *i.p.* glucose compared to $\text{Kiss1}^{\text{Cre}}$ females,
400 indicating that *Stim1*^{kk0} females were more glucose tolerant compared to $\text{Kiss1}^{\text{Cre}}$ controls. *Stim1*^{kk0} females had
401 a significantly higher glucose clearance rate than controls based on the integrated area under the curve (*Stim1*^{kk0}
402 versus the $\text{Kiss1}^{\text{Cre}}$ controls AUC: $20,232 \pm 868$ mg/dL \times min, $n = 6$ versus $22,622 \pm 624$ mg/dL \times min, $n = 6$).
403 Finally, when both groups were euthanized after eight weeks on HFD and the tissues harvested, both the

404 intrascapular brown adipose tissue (iBAT) and perigonadal adipose tissue (GAT) were dissected from each
405 mouse and weighed. Both iBAT and GAT masses were significantly lighter in the *Stim1*^{ko} versus the *Kiss1*^{Cre}
406 females (*Stim1*^{ko} versus the *Kiss1*^{Cre} iBAT: 73.3 ± 6.0 mg, n=10 versus 97.3 ± 9.6 mg, n=10; *Stim1*^{ko} versus
407 the *Kiss1*^{Cre} GAT: 1.5 ± 0.2 g, n=10 versus 2.3 ± 0.2 g, n=10) (**Figures 7F, G**). Overall, these results suggest
408 that conditional deletion of *Stim1* in *Kiss1*^{ARH} neurons affords some protection against diet-induced obesity.
409 However, we cannot overlook the possibility that deletion of *Stim1* in *Kiss1*-expressing hepatocytes might
410 contribute to this metabolic phenotype (Song et al., 2014).

411

412 Discussion

413 For the first time, we show that conditional knockout of *Stim1* significantly reduces store-operated Ca^{2+} entry
414 (SOCE) in *Kiss1*^{ARH} neurons following thapsigargin-mediated depletion of Ca^{2+} stores. Based on single cell
415 qPCR analysis, *Stim1* mRNA was expressed at approximately two-fold higher levels than *Stim2* in *Kiss1*^{ARH}
416 neurons, and deletion of *Stim1* did not alter expression of *Stim2* in *Kiss1*^{ARH} neurons—i.e., there was no
417 developmental compensation. Selective deletion of *Stim1* in *Kiss1*^{ARH} neurons augmented the TacR3-mediated
418 increase in $[\text{Ca}^{2+}]_i$ and synchronous activity of *Kiss1*^{ARH} neurons by almost 4-fold. Whole-cell recording revealed
419 that the slow EPSP induced by high-frequency optogenetic stimulation of *Kiss1*^{ARH}:ChR2 neurons was
420 significantly enhanced by *Stim1* deletion. This augmentation of the slow EPSP was mediated by TacR3 coupling
421 to TRPC 5 channel activation since the senktide-induced inward current was equally enhanced. Moreover, the
422 inward current exhibited the signature double rectifying I/V plot of TRPC 5 channels and was antagonized by the
423 TRPC 4/5 channel blocker HC070. The enhanced TacR3 signaling in *Stim1*^{ko} female mice afforded some
424 protection against diet-induced obesity and glucose intolerance.

425

426 Mammalian TRPC channels can be activated by G protein-coupled receptors and receptor tyrosine kinases
427 (Clapham, 2003; Ambudkar and Ong, 2007) and are one of the major targets for group I metabotropic glutamate
428 receptor (mGluR1) signaling in CNS neurons (Tozzi et al., 2003; Bengtson et al., 2004; Faber et al., 2006; Berg
429 et al., 2007). In substantia nigra dopamine neurons TRPC 5 channels are highly expressed, and mGluR1
430 agonists induce a current that exhibits a double-rectifying current-voltage plot (Tozzi et al., 2003) similar to the

431 effects of the NKB agonist senktide in Kiss1^{ARH} neurons (**Figure 3**). Both mGluR1 and TacR3 are Gq-coupled
432 to phospholipase C (PLC) activation which leads to hydrolysis of phosphatidylinositol 4,5-bisphosphate (PIP₂) to
433 diacylglycerol (DAG) and inositol 1,4,5 triphosphate (IP₃). TRPC channels are minimally Ca²⁺ selective, but can
434 associate with Orai calcium channels to form calcium release-activated calcium channels (Birnbaumer, 2009).
435 A unique feature of TRPC 5 (and TRPC 4) channels is that they are potentiated by lanthanum (La³⁺) (Clapham
436 et al., 2005), which we have exploited to characterize TRPC 5 signaling in POMC neurons (Qiu et al., 2010; Qiu
437 et al., 2014).

438

439 Both leptin and insulin excite/depolarize Kiss1^{ARH} and proopiomelanocortin (POMC) neurons through
440 activation of TRPC 5 channels (Qiu et al., 2010; Qiu et al., 2011; Qiu et al., 2014; Kelly et al., 2018). More
441 recently, we documented a critical role of STIM1 in the insulin signaling cascade in POMC neurons (Qiu et al.,
442 2018b). *Stim1* mRNA is highly expressed in POMC (Qiu et al., 2018b) and Kiss1^{ARH} neurons (**Figure 1**), and E2
443 downregulates *Stim1* mRNA expression in microdissected arcuate nuclei that encompasses these two
444 populations of neurons. Downregulation of *Stim1* is critical for maintaining insulin excitability in POMC neurons
445 with diet-induced obesity (Qiu et al., 2018b). In ovariectomized females that are relatively refractory to insulin
446 excitation, pharmacological blockade of the SOCE complex quickly increases the insulin-mediated excitation of
447 POMC neurons (*i.e.*, activation of the TRPC 5 mediated inward current), which supports the concept that TRPC
448 5 channels play a role both in SOCE and receptor operated calcium entry (Birnbaumer, 2009; Salido et al., 2011).
449 Therefore, selective deletion of *Stim1* in Kiss1 neurons should ensure that TRPC 5 channels function as receptor-
450 operated channels to couple TacR3's and transmit the excitatory effects of NKB to induce synchronous firing of
451 Kiss1^{ARH} neurons as demonstrated in the present findings.

452

453 Downregulating STIM1 inhibits SOCE, attenuates Ca²⁺ influx into the ER and elevates intracellular Ca²⁺
454 levels, which could also contribute to activation of TRPC5 channels in Kiss1^{ARH} neurons (Blair et al., 2009).
455 Indeed, we have found that Ca²⁺ greatly potentiates the leptin-induced TRPC 5 current in POMC neurons (Qiu
456 et al., 2010). In cortical neurons and heterologous cells expressing Cav1.2 (L-type calcium) channels and *Stim1*,
457 inhibition of STIM1 augments Ca²⁺ influx through L-type calcium channels (Park et al., 2010; Wang et al., 2010).

458 Calcium sensing by STIM1 is also involved in the control of L-type Ca^{2+} channel activity in the hippocampal
459 pyramidal neurons such that glutamate-mediated depolarization activates L-type calcium channels, and releases
460 Ca^{2+} from ER stores that activates STIM1 and drives aggregation of the L-type calcium channels to inhibit their
461 activity (Dittmer et al., 2017). Quite possibly in $\text{Kiss1}^{\text{ARH}}$ neurons and Purkinje cells (Ryu et al., 2017) deletion
462 of *Stim1* allows the “dis-aggregation” of TRPC 5 channels, which is reflected in the significant decrease in R_{in} in
463 both cell types with deletion. Furthermore, knocking down STIM1 in cardiomyocyte-derived (HL-1) cells
464 increases the peak amplitude and current density of T-type calcium channels and shifts the activation curve
465 toward more negative membrane potentials (Nguyen et al., 2013). Biotinylation assays reveal that knocking
466 down *Stim1* increases T-type calcium channel surface expression, and co-immunoprecipitation assays suggest
467 that STIM1 directly regulates T-type channel activity (Nguyen et al., 2013). Thus, STIM1 appears to be a negative
468 regulator of voltage-gated calcium channel activity. On the other hand, estradiol treatment in ovariectomized
469 females upregulates Cav3.1 channel expression by 3-fold and whole cell currents by 10-fold in $\text{Kiss1}^{\text{ARH}}$ neurons,
470 which greatly enhances the excitability and contributes to the synchronous firing of $\text{Kiss1}^{\text{ARH}}$ neurons (Qiu et al.,
471 2018a). The T-type calcium channel Cav3.1 underlies burst firing in rostral hypothalamic kisspeptin neurons
472 (Zhang et al., 2013b) and facilitates TRPC 4 channel activation in GnRH neurons (Zhang et al., 2008; Zhang et
473 al., 2013a). Cav3.1 channels may also facilitate TRPC5 channel opening in $\text{Kiss1}^{\text{ARH}}$ neurons (**Figure 8**), but
474 this remains to be determined.

475

476 Presumably with conditional knockout, *Stim1* was deleted in all cells expressing kisspeptin, which includes
477 arcuate, anteroventral periventricular preoptic (AVPV) and amygdala kisspeptin neurons, and non-neural
478 kisspeptin cells in the gonads, pancreas and liver (Dudek et al., 2019). Currently, we found that the deletion of
479 *Stim1* in kisspeptin neurons had a minor effect on the estrous cycle. $\text{Stim1}^{\text{kko}}$ mice exhibited more estrous-type
480 vaginal cytology, which may be indicative of higher levels of circulating estrogens due to increased synchronous
481 firing of kisspeptin neurons and excitatory drive to GnRH neurons (Qiu et al., 2016; Clarkson et al., 2017). It is
482 important to note that synchronous firing of “pulse generator” $\text{Kiss1}^{\text{ARH}}$ neurons is a failsafe system for
483 maintaining gonadotropin pulses and folliculogenesis in female rodents (Nagae et al., 2021).

484

485 Because of the well-documented anorexigenic actions of E2 on POMC and Agouti-related peptide
486 (AgRP) neurons controlling energy homeostasis (Qiu et al., 2006; Roepke et al., 2010; Clegg, 2012; Kelly and
487 Rønnekleiv, 2012; Smith et al., 2013), we ovariectomized the females before feeding them a high fat diet. After
488 7 weeks on a high fat diet, *Stim1*^{kk0} females gained modestly less body weight but showed significantly less body
489 fat and lean mass than ovariectomized *Kiss1*^{Cre} females on a high fat diet. Most importantly, *Stim1*^{kk0} females
490 exhibited improved glucose tolerance. *Kiss1*^{ARH} neurons probably mediate these protective effects via their input
491 onto POMC and AgRP neurons. Besides the peptides *Kiss1*^{ARH} neurons also co-express the vesicular glutamate
492 transporter 2 (vGluT2) (Cravo et al., 2011), and we have documented that optogenetic stimulation of *Kiss1*^{ARH}
493 neurons expressing channelrhodopsin releases glutamate, which is dependent on the estrogenic state of
494 females (Qiu et al., 2018a). Although the mRNA expression of *Kiss1*, *Tac2* and *Pdyn* mRNA in *Kiss1*^{ARH} neurons
495 are all down-regulated by E2 (Navarro et al., 2009; Lehman et al., 2010), *Vglut2* mRNA expression is upregulated
496 together with increased probability of glutamate release in E2 treated, ovariectomized females (Qiu et al.,
497 2018a). Low frequency (1-2 Hz) optogenetic stimulation of *Kiss1*^{ARH} neurons evokes fast ionotropic
498 glutamatergic EPSCs in POMC and AgRP neurons, but high frequency (20 Hz) optogenetic stimulation releases
499 enough glutamate to induce a slow excitatory response in POMC neurons but a slow inhibitory response in AgRP
500 neurons (Nestor et al., 2016; Qiu et al., 2016; Qiu et al., 2018a). Indeed, the group I mGluR agonist DHPG
501 depolarizes POMC neurons, while group II/III mGluR agonists (DCG-IV; AMN082) hyperpolarize AgRP neurons
502 (Qiu et al., 2018a). Group I mGluRs (mGluR1 and mGluR5) are G_q/G₁₁-coupled, while group II/III mGluRs
503 (mGluR2 and mGluR7) are G_i/G_o-coupled (Niswender and Conn, 2010). Hence, the output of *Kiss1*^{ARH} neurons
504 excites the anorexigenic POMC neurons and inhibits the orexigenic AgRP neurons. Therefore, *Kiss1*^{ARH} neurons
505 appear to be an integral part of an anorexigenic circuit in the hypothalamus (Qiu et al., 2018a; Rønnekleiv et al.,
506 2019; Navarro, 2020).

507
508 Presently, there is compelling evidence that *Kiss1*^{ARH} neurons are a critical “command” neuron for
509 coordinating energy states with reproductive functions (see (Rønnekleiv et al., 2019; Navarro, 2020) for review).
510 We have now documented that conditional knockout of *Stim1* in *Kiss1*^{ARH} neurons, which augments the NKB-
511 mediated depolarization of these neurons via TRPC 5 channels, helps protect ovariectomized, female mice from

512 diet-induced obesity and glucose intolerance. In addition, in preliminary experiments we have found that insulin
513 treatment *in vitro* increases the synchronous firing (GCaMP6 activity) of Kiss1^{ARH} neurons, which further
514 emphasizes its role as a “command” neuron. Clearly, Kiss1^{ARH} neurons are part of a hypothalamic circuit for
515 coordinating reproduction with energy balance, but additional experiments are needed to elucidate the cellular
516 mechanisms by which steroid and metabolic hormonal signaling synergize to govern their activity.

517

518 **References**

519

520 Ambudkar IS, Ong HL (2007) Organization and function of TRPC channelsomes. *Pflügers Archiv: European*
521 *Journal of Physiology* 455:187-200.

522 Asarian L, Geary N (2006) Modulation of appetite by gonadal steroid hormones. *Philosophical Transactions of*
523 *the Royal Society B: Biological Sciences* 361:1251-1263.

524 Ayala JE, Samuel VT, Morton GJ, Obici S, Croniger CM, Shulman GI, Wasserman DH, McGuinness OP,
525 Consortium NIHMMPC (2010) Standard operating procedures for describing and performing metabolic
526 tests of glucose homeostasis in mice. *Disease Models & Mechanisms* 3:525-534.

527 Bengtson CP, Tozzi A, Bernardi G, Mercuri NB (2004) Transient receptor potential-like channels mediate
528 metabotropic glutamate receptor EPSCs in rat dopamine neurones. *The Journal of Physiology* 555:323-
529 330.

530 Berg AP, Sen N, Bayliss DA (2007) TrpC3/C7 and Slo2.1 are molecular targets for metabotropic glutamate
531 receptor signaling in rat striatal cholinergic interneurons. *The Journal of Neuroscience* 27:8845-8856.

532 Berna-Erro A, Braun A, Kraft R, Kleinschmitz C, Schuhmann MK, Stegner D, Wultsch T, Eilers J, Meuth SG,
533 Stoll G, Nieswandt B (2009) STIM2 Regulates Capacitive Ca²⁺ Entry in Neurons and Plays a Key Role
534 in Hypoxic Neuronal Cell Death. *Science Signaling* 2:ra67-ra67.

535 Birnbaumer L (2009) The TRPC class of ion channels: a critical review of their roles in slow, sustained
536 increases in intracellular Ca²⁺ concentrations. *Annual Review of Pharmacology and Toxicology* 49:395-
537 426.

538 Blair NT, Kaczmarek JS, Clapham DE (2009) Intracellular calcium strongly potentiates agonist-activated

- 539 TRPC5 channels. *The Journal of General Physiology* 133:525-546.
- 540 Bosch MA, Tonsfeldt KJ, Rønnekleiv OK (2013) mRNA expression of ion channels in GnRH neurons: subtype-
541 specific regulation by 17 β -Estradiol. *Molecular and Cellular Endocrinology* 367:85-97.
- 542 Brini M, Calì T, Ottolini D, Carafoli E (2014) Neuronal calcium signaling: function and dysfunction. *Cellular and*
543 *Molecular Life Sciences* 71:2787-2814.
- 544 Castellano JM, Tena-Sempere M (2013) Metabolic regulation of kisspeptin. *Advances in Experimental*
545 *Medicine and Biology* 784:363-383.
- 546 Castellano JM, Navarro VM, Fernández-Fernández R, Nogueiras R, Tovar S, Roa J, Vazquez MJ, Vigo E,
547 Casanueva FF, Aguilar E, Pinilla L, Dieguez C, Tena-Sempere M (2005) Changes in hypothalamic
548 KiSS-1 system and restoration of pubertal activation of the reproductive axis by kisspeptin in
549 undernutrition. *Endocrinology* 146:3917-3925.
- 550 Clapham DE (2003) TRP channels as cellular sensors. *Nature* 426:517-524.
- 551 Clapham DE, Julius D, Montell C, Schultz G (2005) International Union of Pharmacology. XLIX. Nomenclature
552 and structure-function relationships of transient receptor potential channels. *Pharmacological Reviews*
553 57:427-450.
- 554 Clarkson J, Han SY, Piet R, McLennan T, Kane GM, Ng J, Porteous RW, Kim JS, Colledge WH, Iremonger KJ,
555 Herbison AE (2017) Definition of the hypothalamic GnRH pulse generator in mice. *Proceedings of the*
556 *National Academy of Sciences of the United States of America* 114:E10216-E10223.
- 557 Clegg DJ (2012) Minireview: the year in review of estrogen regulation of metabolism. *Molecular Endocrinology*
558 26:1957-1960.
- 559 Cravo RM, Margatho LO, Osborne-Lawrence S, Donato JJ, Atkin S, Bookout AL, Rovinsky S, Frazão R, Lee
560 CE, Gautron L, Zigman JM, Elias CF (2011) Characterization of *Kiss1* neurons using transgenic mouse
561 models. *Neuroscience* 173:37-56.
- 562 Czaja JA (1978) Ovarian influences on primate food intake: assessment of progesterone actions. *Physiology &*
563 *Behavior* 21:923-928.
- 564 d'Anglemont de Tassigny X, Fagg LA, Dixon JPC, Day K, Leitch HG, Hendrick AG, Zahn D, Franceschini I,
565 Caraty A, Carlton MBL, Aparicio SAJR, Colledge WH (2007) Hypogonadotropic hypogonadism in mice

- 566 lacking a functional *KiSS 1* gene. *Proceedings of the National Academy of Sciences of the United*
567 *States of America* 104:10714-10719.
- 568 De Bond JA, Smith JT (2014) Kisspeptin and energy balance in reproduction. *Reproduction* 147:R53-63.
- 569 de Croft S, Boehm U, Herbison AE (2013) Neurokinin B activates arcuate kisspeptin neurons through multiple
570 tachykinin receptors in the male mouse. *Endocrinology* 154:2750-2760.
- 571 De Roux N, Genin E, Carel J-C, Matsuda F, Chaussain J-L, Milgrom E (2003) Hypogonadotropic
572 hypogonadism due to loss of function of the *KiSS 1*-derived peptide receptor GPR54. *Proceedings of*
573 *the National Academy of Sciences of the United States of America* 100:10972-10976.
- 574 Dittmer PJ, Wild AR, Dell'Acqua ML, Sather WA (2017) STIM1 Ca^{2+} Sensor Control of L-type Ca^{2+} -Channel-
575 Dependent Dendritic Spine Structural Plasticity and Nuclear Signaling. *Cell Reports* 19:321-334.
- 576 Dudek M, Ziarniak K, Cateau M-L, Dufourny L, Sliwowska JH (2019) Diabetes type 2 and kisspeptin: Central
577 and peripheral sex-specific actions. *Trends in Endocrinology & Metabolism* 30:833-843.
- 578 Faber ES, Sedlak P, Vidovic M, Sah P (2006) Synaptic activation of transient receptor potential channels by
579 metabotropic glutamate receptors in the lateral amygdala. *Neuroscience* 137:781-794.
- 580 Fernández-Fernández R, Martini AC, Navarro VM, Castellano JM, Dieguez C, Aguilar E, Pinilla L, Tena-
581 Sempere M (2006) Novel signals for the integration of energy balance and reproduction. *Molecular and*
582 *Cellular Endocrinology* 254-255:127-132.
- 583 Fu LY, van den Pol AN (2010) Kisspeptin directly excites anorexigenic proopiomelanocortin neurons but
584 inhibits orexigenic neuropeptide Y cells by an indirect synaptic mechanism. *The Journal of*
585 *Neuroscience* 30:10205-10219.
- 586 Gao Y, Yao T, Deng Z, Sohn J-W, Sun J, Huang Y, Kong X, Yu K-J, Wang R-T, Chen H, Guo H, Yan J,
587 Cunningham KA, Chang Y, Liu T, Williams KW (2017) TrpC5 mediates acute leptin and serotonin
588 effects via *Pomc* neurons. *Cell Reports* 18:583-592.
- 589 Goodman RL, Lehman MN, Smith JT, Coolen LM, de Oliveira CVR, Jafarzadehshirazi MR, Pereira A, Iqbal J,
590 Caraty A, Ciofi P, Clarke IJ (2007) Kisspeptin neurons in the arcuate nucleus of the ewe express both
591 dynorphin A and neurokinin B. *Endocrinology* 148:5752-5760.
- 592 Gruszczynska-Biegala J, Pomorski P, Wisniewska MB, Kuznicki J (2011) Differential Roles for STIM1 and

- 593 STIM2 in Store-Operated Calcium Entry in Rat Neurons. PLOS ONE 6:e19285.
- 594 Guner G, Guzelsoy G, Isleyen FS, Sahin GS, Akkaya C, Bayam E, Kotan EI, Kabakcioglu A, Ince-Dunn G
595 (2017) NEUROD2 Regulates *Stim1* Expression and Store-Operated Calcium Entry in Cortical Neurons.
596 *eneuro* 4:ENEURO.0255-0216.2017.
- 597 Han S-K, Gottsch ML, Lee KJ, Popa SM, Smith JT, Jakawich SK, Clifton DK, Steiner RA, Herbison AE (2005)
598 Activation of gonadotropin-releasing hormone neurons by kisspeptin as a neuroendocrine switch for the
599 onset of puberty. *The Journal of Neuroscience* 25:11349-11356.
- 600 Hartmann J, Karl RM, Alexander RP, Adelsberger H, Brill MS, Rühlmann C, Ansel A, Sakimura K, Baba Y,
601 Kuroasaki T, Misgeld T, Konnerth A (2014) STIM1 controls neuronal Ca^{2+} signaling, mGluR1-dependent
602 synaptic transmission, and cerebellar motor behavior. *Neuron* 82:635-644.
- 603 Just S et al. (2018) Treatment with HC-070, a potent inhibitor of TRPC4 and TRPC5, leads to anxiolytic and
604 antidepressant effects in mice. *PLOS One* 13:e0191225.
- 605 Kelly MJ, Rønneklev OK (2012) Membrane-initiated actions of estradiol that regulate reproduction, energy
606 balance and body temperature. *Frontiers in Neuroendocrinology* 33:376-387.
- 607 Kelly MJ, Qiu J, Rønneklev OK (2018) TRPCing around the hypothalamus. *Frontiers in Neuroendocrinology*
608 51:116-124.
- 609 Kuohung W, Kaiser UB (2006) GPR54 and KiSS-1: role in the regulation of puberty and reproduction. *Reviews*
610 in *Endocrine and Metabolic Disorders* 7:257-263.
- 611 Lehman MN, Coolen LM, Goodman RL (2010) Minireview: kisspeptin/neurokinin B/dynorphin (KNDy) cells of
612 the arcuate nucleus: a central node in the control of gonadotropin-releasing hormone secretion.
613 *Endocrinology* 151:3479-3489.
- 614 Livak KJ, Schmittgen TD (2001) Analysis of relative gene expression data using real-time quantitative PCR
615 and the $2^{-\Delta\Delta CT}$ method. *Methods* 25:402-408.
- 616 Madisen L et al. (2012) A toolbox of Cre-dependent optogenetic transgenic mice for light-induced activation
617 and silencing. *Nature Neuroscience* 15:793-802.
- 618 Mayer C, Acosta-Martinez M, Dubois SL, Wolfe A, Radovick S, Boehm U, Levine JE (2010) Timing and
619 completion of puberty in female mice depend on estrogen receptor α -signaling in kisspeptin neurons.

- 620 Proceedings of the National Academy of Sciences 107:22693-22698.

621 Moccia F, Zuccolo E, Soda T, Tanzi F, Guerra G, Mapelli L, Lodola F, D'Angelo E (2015) Stim and Orai
622 proteins in neuronal Ca^{2+} signaling and excitability. *Frontiers in Cellular Neuroscience* 9:153.

623 Nagae M, Uenoyama Y, Okamoto S, Tsuchida H, Ikegami K, Goto T, Majarune S, Nakamura S, Sanbo M,
624 Hirabayashi M, Kobayashi K, Inoue N, Tsukamura H (2021) Direct evidence that KNDy neurons
625 maintain gonadotropin pulses and folliculogenesis as the GnRH pulse generator. *Proceedings of the
626 National Academy of Sciences* 118:e2009156118.

627 Navarro VM (2020) Metabolic regulation of kisspeptin — the link between energy balance and reproduction.
628 *Nature Reviews Endocrinology* 16:407-420.

629 Navarro VM, Gottsch ML, Chavkin C, Okamura H, Clifton DK, Steiner RA (2009) Regulation of gonadotropin-
630 releasing hormone secretion by kisspeptin/dynorphin/neurokinin B neurons in the arcuate nucleus of
631 the mouse. *The Journal of Neuroscience* 29:11859-11866.

632 Navarro VM, Castellano JM, McConkey SM, Pineda R, Ruiz-Pino F, Pinilla L, Clifton DK, Tena-Sempere M,
633 Steiner RA (2011) Interactions between kisspeptin and neurokinin B in the control of GnRH secretion in
634 the female rat. *American Journal of Physiology: Endocrinology and Metabolism* 300:E202-E210.

635 Nestor CC, Kelly MJ, Rønnekleiv OK (2014) Cross-talk between reproduction and energy homeostasis: central
636 impact of estrogens, leptin and kisspeptin signaling. *Hormone Molecular Biology and Clinical
637 Investigation* 17:109-128.

638 Nestor CC, Qiu J, Padilla SL, Zhang C, Bosch MA, Fan W, Aicher SA, Palmiter RD, Rønnekleiv OK, Kelly MJ
639 (2016) Optogenetic stimulation of arcuate nucleus Kiss1 neurons reveals a steroid-dependent
640 glutamatergic input to POMC and AgRP neurons in male mice. *Molecular Endocrinology* 30:630-644.

641 Nguyen N, Biet M, Simard É, Béliveau É, Francoeur N, Guillemette G, Dumaine R, Grandbois M, Boulay G
642 (2013) STIM1 participates in the contractile rhythmicity of HL-1 cells by moderating T-type Ca^{2+} channel
643 activity. *Biochimica et Biophysica Acta* 1833:1294-1303.

644 Niswender CM, Conn PJ (2010) Metabotropic glutamate receptors: physiology, pharmacology, and disease.
645 *Annual Review of Pharmacology and Toxicology* 50:295-322.

646 Oh-hora M, Yamashita M, Hogan PG, Sharma S, Lamperti E, Chung W, Prakriya M, Feske S, Rao A (2008)

- 647 Dual functions for the endoplasmic reticulum calcium sensors STIM1 and STIM2 in T cell activation and
648 tolerance. *Nature Immunology* 9:432-443.
- 649 Okamura H, Tsukamura H, Ohkura S, Uenoyama Y, Wakabayashi Y, Maeda K (2013) Kisspeptin and GnRH
650 pulse generation. *Advances in Experimental Medicine and Biology* 784:297-323.
- 651 Padilla SL, Johnson CW, Barker FD, Patterson MA, Palmiter RD (2018) A neural circuit underlying the
652 generation of hot flushes. *Cell Reports* 24:271-277.
- 653 Park CY, Shcheglovitov A, Dolmetsch R (2010) The CRAC channel activator STIM1 binds and inhibits L-type
654 voltage-gated calcium channels. *Science* 330:101-105.
- 655 Pavez M, Thompson AC, Arnott HJ, Mitchell CB, D'Atri I, Don EK, Chilton JK, Scott EK, Lin JY, Young KM,
656 Gasperini RJ, Foa L (2019) STIM1 Is Required for Remodeling of the Endoplasmic Reticulum and
657 Microtubule Cytoskeleton in Steering Growth Cones. *The Journal of Neuroscience* 39:5095-5114.
- 658 Pfaffl MW (2001) A new mathematical model for relative quantification in real-time RT-PCR. *Nucleic Acids
659 Research* 29:e45.
- 660 Pielecka-Fortuna J, Chu Z, Moenter SM (2008) Kisspeptin acts directly and indirectly to increase gonadotropin-
661 releasing hormone neuron activity and its effects are modulated by estradiol. *Endocrinology* 149:1979-
662 1986.
- 663 Qiu J, Fang Y, Rønneklev OK, Kelly MJ (2010) Leptin excites proopiomelanocortin neurons via activation of
664 TRPC channels. *The Journal of Neuroscience* 30:1560-1565.
- 665 Qiu J, Fang Y, Bosch MA, Rønneklev OK, Kelly MJ (2011) Guinea pig kisspeptin neurons are depolarized by
666 leptin via activation of TRPC channels. *Endocrinology* 152:1503-1514.
- 667 Qiu J, Bosch MA, Tobias SC, Grandy DK, Scanlan TS, Rønneklev OK, Kelly MJ (2003) Rapid signaling of
668 estrogen in hypothalamic neurons involves a novel G-protein-coupled estrogen receptor that activates
669 protein kinase C. *The Journal of Neuroscience* 23:9529-9540.
- 670 Qiu J, Nestor CC, Zhang C, Padilla SL, Palmiter RD, Kelly MJ, Rønneklev OK (2016) High-frequency
671 stimulation-induced peptide release synchronizes arcuate kisspeptin neurons and excited GnRH
672 neurons. *eLife* 5:e16246.
- 673 Qiu J, Rivera HM, Bosch MA, Padilla SL, Stincic TL, Palmiter RD, Kelly MJ, Rønneklev OK (2018a)

- 674 Estrogenic-dependent glutamatergic neurotransmission from kisspeptin neurons governs feeding
675 circuits in females. *eLife* 7:e35656.

676 Qiu J, Bosch MA, Meza C, Navarro UV, Nestor CC, Wagner EJ, Rønnekleiv OK, Kelly MJ (2018b) Estradiol
677 protects proopiomelanocortin neurons against insulin resistance. *Endocrinology* 159:647-664.

678 Qiu J, Zhang C, Borgquist A, Nestor CC, Smith AW, Bosch MA, Ku S, Wagner EJ, Rønnekleiv OK, Kelly MJ
679 (2014) Insulin excites anorexigenic proopiomelanocortin neurons via activation of canonical transient
680 receptor potential channels. *Cell Metabolism* 19:682-693.

681 Qiu J, Bosch MA, Tobias SC, Krust A, Graham S, Murphy S, Korach KS, Chambon P, Scanlan TS, Rønnekleiv
682 OK, Kelly MJ (2006) A G-protein-coupled estrogen receptor is involved in hypothalamic control of
683 energy homeostasis. *The Journal of Neuroscience* 26:5649-5655.

684 Roepke TA, Bosch MA, Rick EA, Lee B, Wagner EJ, Seidlova-Wuttke D, Wuttke W, Scanlan TS, Rønnekleiv
685 OK, Kelly MJ (2010) Contribution of a membrane estrogen receptor to the estrogenic regulation of body
686 temperature and energy homeostasis. *Endocrinology* 151:4926-4937.

687 Rønnekleiv OK, Qiu J, Kelly MJ (2019) Arcuate Kisspeptin Neurons Coordinate Reproductive Activities with
688 Metabolism. *Seminars in Reproductive Medicine* 37:131-140.

689 Ruka KA, Burger LL, Moenter SM (2013) Regulation of arcuate neurons coexpressing kisspeptin, neurokinin B,
690 and dynorphin by modulators of neurokinin 3 and κ-opioid receptors in adult male mice. *Endocrinology*
691 154:2761-2771.

692 Ryu C, Jang DC, Jung D, Kim YG, Shim HG, Ryu H-H, Lee Y-S, Linden DJ, Worley PF, Kim SJ (2017) STIM1
693 regulates somatic Ca^{2+} signals and intrinsic firing properties of cerebellar Purkinje neurons. *The Journal*
694 of *Neuroscience* 37:8876.

695 Salido GM, Jardin I, Rosado JA (2011) The TRPC ion channels: association with Orai1 and STIM1 proteins
696 and participation in capacitative and non-capacitative calcium entry. *Advances in Experimental*
697 *Medicine and Biology* 704:413-433.

698 Seminara SB, Messager S, Chatzidaki EE, Thresher RR, Acierno JS, Shagoury JK, Bo-Abbas Y, Kuohung W,
699 Schwinof KM, Hendrick AG, Zahn D, Dixon J, Kaiser UB, Slaugenhaupt SA, Gusella JF, O'Rahilly S,
700 Carlton MBL, Crowley WF, Aparicio SAJR, Colledge WH (2003) The GPR54 gene as a regulator of

- 701 puberty. *The New England Journal of Medicine* 349:1614-1627.
- 702 Smith AW, Bosch MA, Wagner EJ, Rønneklev OK, Kelly MJ (2013) The membrane estrogen receptor ligand
703 STX rapidly enhances GABAergic signaling in NPY/AgRP neurons: Role in mediating the anorexigenic
704 effects of 17 β -estradiol. *American Journal of Physiology: Endocrinology and Metabolism* 305:E632-
705 E640.
- 706 Somasundaram A, Shum AK, McBride HJ, Kessler JA, Feske S, Miller RJ, Prakriya M (2014) Store-Operated
707 CRAC Channels Regulate Gene Expression and Proliferation in Neural Progenitor Cells. *The Journal of*
708 *Neuroscience* 34:9107-9123.
- 709 Song WJ, Mondal P, Wolfe A, Alonso LC, Stamateris R, Ong BW, Lim OC, Yang KS, Radovick S, Novaira HJ,
710 Farber EA, Farber CR, Turner SD, Hussain MA (2014) Glucagon regulates hepatic kisspeptin to impair
711 insulin secretion. *Cell Metabolism* 19:667-681.
- 712 Stengel A, Wang L, Goebel-Stengel M, Tache Y (2011) Centrally injected kisspeptin reduces food intake by
713 increasing meal intervals in mice. *Neuroreport* 22:253-257.
- 714 Sun Y, Zhang H, Selvaraj S, Sukumaran P, Lei S, Birnbaumer L, Singh BB (2017) Inhibition of L-Type Ca²⁺
715 channels by TRPC1-STIM1 complex is essential for the protection of dopaminergic neurons. *The*
716 *Journal of Neuroscience* 37:3364-3377.
- 717 Tolson KP, Marooki N, Wolfe A, Smith JT, Kauffman AS (2019) Cre/lox generation of a novel whole-body
718 Kiss1r KO mouse line recapitulates a hypogonadal, obese, and metabolically-impaired phenotype.
719 *Molecular and Cellular Endocrinology* 498:110559.
- 720 Tolson KP, Garcia C, Yen S, Simonds S, Stefanidis A, Lawrence A, Smith JT, Kauffman AS (2014) Impaired
721 kisspeptin signaling decreases metabolism and promotes glucose intolerance and obesity. *Journal of*
722 *Clinical Investigation* 124:3075-3079.
- 723 Topaloglu AK, Tello JA, Kotan LD, Ozbek MN, Yilmaz MB, Erdogan S, Gurbuz F, Temiz F, Millar RP, Yuksel B
724 (2012) Inactivating KISS1 mutation and hypogonadotropic hypogonadism. *The New England Journal of*
725 *Medicine* 366:629-635.
- 726 Tozzi A, Bengtson CP, Longone P, Carignani C, Fusco FR, Bernardi G, Mercuri NB (2003) Involvement of
727 transient receptor potential-like channels in responses to mGluR-I activation in midbrain dopamine

- 728 neurons. European Journal of Neuroscience 18:2133-2145.
- 729 Wang Y, Deng X, Mancarella S, Hendron E, Eguchi S, Soboloff J, Tang XD, Gill DL (2010) The calcium store
730 sensor, STIM1, reciprocally controls Orai and Cav1.2 channels. Science 330:105-109.
- 731 Yuan JP, Zeng W, Huang GN, Worley PF, Muallem S (2007) STIM1 heteromultimerizes TRPC channels to
732 determine their function as store-operated channels. Nature Cell Biology 9:636-645.
- 733 Zhang C, Roepke TA, Kelly MJ, Rønnekleiv OK (2008) Kisspeptin depolarizes gonadotropin-releasing
734 hormone neurons through activation of TRPC-like cationic channels. The Journal of Neuroscience
735 28:4423-4434.
- 736 Zhang C, Bosch MA, Rønnekleiv OK, Kelly MJ (2013a) Kisspeptin activation of TRPC4 channels in female
737 GnRH neurons requires PIP₂ depletion and cSrc kinase activation. Endocrinology 154:2772-2783.
- 738 Zhang C, Tonsfeldt KJ, Qiu J, Bosch MA, Kobayashi K, Steiner RA, Kelly MJ, Rønnekleiv OK (2013b)
739 Molecular mechanisms that drive estradiol-dependent burst firing of Kiss1 neurons in the rostral
740 periventricular preoptic area. American Journal of Physiology: Endocrinology and Metabolism
741 305:E1384-E1397.
- 742
- 743

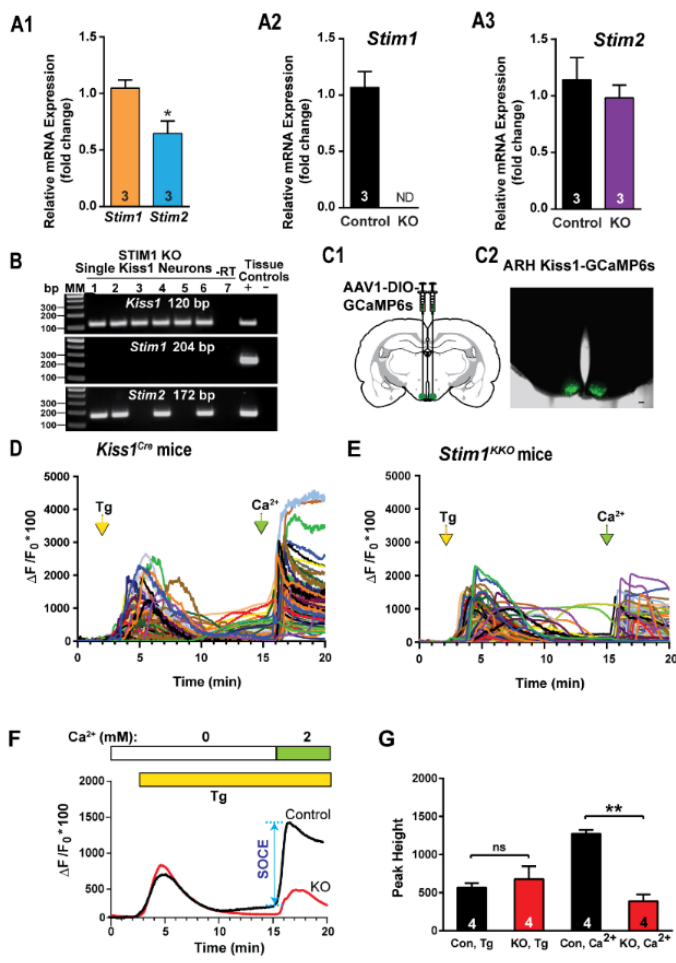
744

Figure Legends

745

746

FIGURE 1



747

748

749

750

751

752

753

754

755

756

757

758

759

760

761

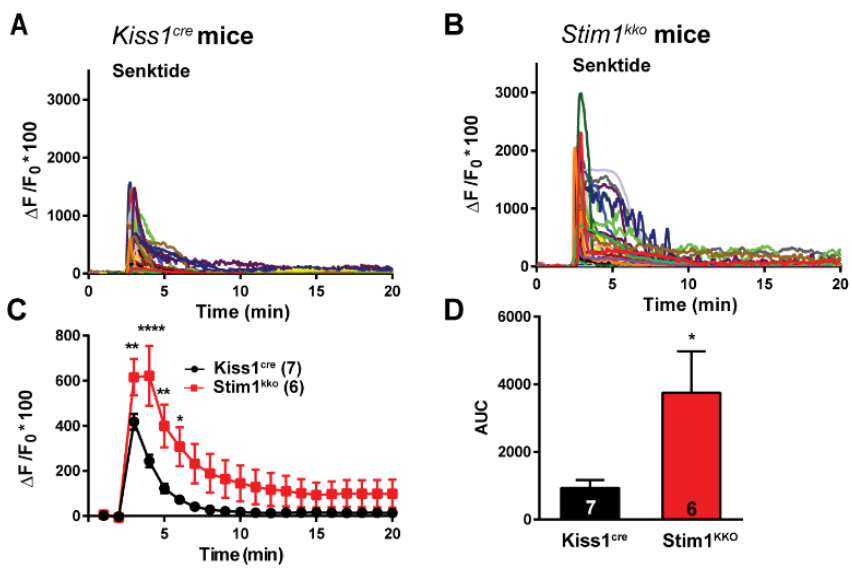
762

Figure 1. Expression Patterns of *Stim1* and *2* in the arcuate Kiss1 neurons. A1-A3, quantitative PCR assay measuring *Stim1* and *Stim2* in *Kiss1^{ARH}* neuronal pools (n = 3 animals, 10 cells in each pool, 4 pools/animal) from *Kiss1^{Cre}* control and *Stim1^{KKO}* female mice (n=3 animals per group). **A1**, comparison between *Stim1* and *Stim2* in controls only. Bar graphs represent mean \pm SEM (Unpaired t-test, $t_{(4)} = 3.079$, * $p = 0.0370$); **A2**, *Stim1* was non-detectable (ND) in the *STIM1^{KKO}* neuronal pools (Unpaired t-test, $t_{(4)} = 7.559$, ** $p = 0.0016$); **A3**, the *Stim2* expression level of *Kiss1^{ARH}* neurons was not different between *Kiss1^{Cre}* control and *Stim1^{KKO}* female mice (Unpaired t-test, $t_{(4)} = 0.7143$, $p = 0.5145$). **B**, representative gels illustrating mRNA expression of *Stim1* and *Stim2* in single *Kiss1^{ARH}* neurons from *Stim1^{KKO}* mice. The expected base pair (bp) sizes are *Kiss1*, 120 bp; *Stim1*, 204 bp; *Stim2*, 172 bp. A single neuron was processed without reverse transcriptase (-RT) and RNA extracted

771 from hypothalamic tissue was used as positive (+, with RT) and negative (-, without RT) tissue controls. MM,
772 molecular marker. **C**, left, schematic of a coronal section showing the bilateral viral injections in the ARH with
773 AAV-DIO-GCaMP6s. Right, photomicrograph showing a coronal section confirming targeted bilateral injections
774 of DIO-GCaMP6s into the ARH. **D** and **E**, representative traces of GCaMP6s activity based on cytosolic Ca^{2+}
775 measurements in $\text{Kiss1}^{\text{ARH}}$ neurons from $\text{Kiss1}^{\text{Cre}}:\text{GCaMP6s}$ mice (D) and $\text{Stim1}^{\text{KKO}}:\text{GCaMP6s}$ mice (E). ER Ca^{2+}
776 stores were depleted with 2 μM thapsigargin, a SERCA inhibitor, after 20 min of perfusion with aCSF containing
777 0 mM Ca^{2+} . SOCE was evaluated by substituting the extracellular aCSF containing 0 mM Ca^{2+} with aCSF
778 containing 2 mM Ca^{2+} . **F**, averaged traces from D and E revealed that deletion of Stim1 in $\text{Kiss1}^{\text{ARH}}$ neurons
779 attenuated the store-operated Ca^{2+} entry (SOCE). **G**, bar graphs summarizing the effects of depletion of Ca^{2+}
780 store by Tg and Ca^{2+} influx (SOCE) in $\text{Kiss1}^{\text{ARH}}$ neurons from $\text{Kiss1}^{\text{Cre}}:\text{GCaMP6s}$ and $\text{Stim1}^{\text{KKO}}:\text{GCaMP6s}$ mice
781 (two-way ANOVA: main effect of treatment ($F_{(1,3)} = 13.84$, $p = 0.0338$), main effect of time ($F_{(1,3)} = 5.199$, $p =$
782 0.1069) and interaction ($F_{(1,3)} = 52.14$, $p = 0.0055$); n = number of slices; *post hoc* Bonferroni test, ** $p < 0.01$, for
783 SOCE; ns = no significant, for depletion of Ca^{2+} store.

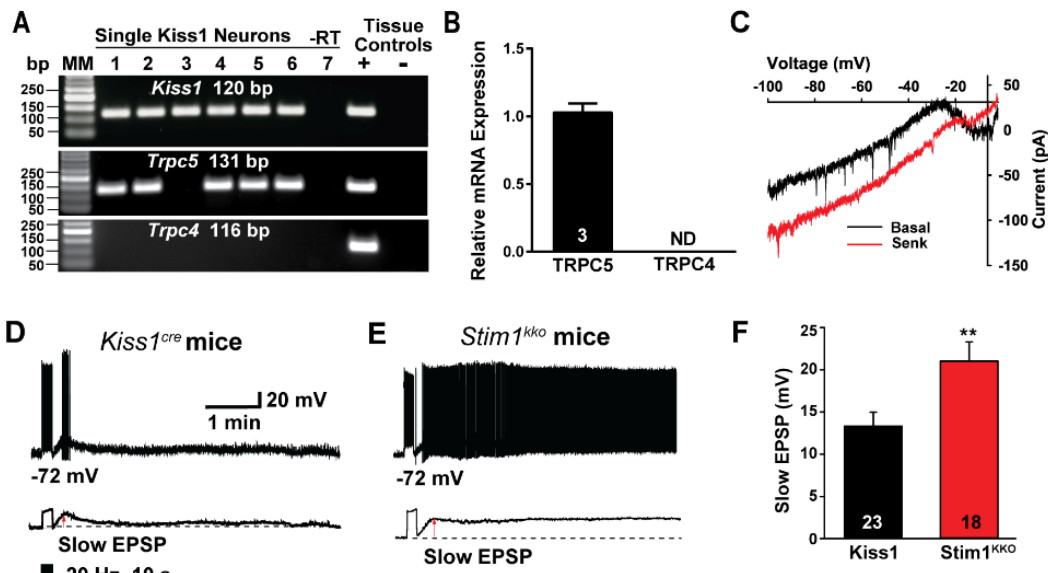
784

785 FIGURE 2



798 in Kiss1^{ARH} neurons from *Kiss1*^{Cre} (A) and *Stim1*^{kko} (B) mice. Traces represent individual cells within a single
 799 slice. **C**, summary of the potentiation of senktide-induced $[Ca^{2+}]_i$ by deletion of *Stim1*. Two-way ANOVA: main
 800 effect of treatment ($F_{(1,11)} = 5.265, p = 0.0424$), main effect of time ($F_{(19,209)} = 42.69, p < 0.0001$) and interaction
 801 ($F_{(19,209)} = 6.486, p < 0.0001$); n = number of slices; *post hoc* Bonferroni test, *** $p < 0.001$; ** $p < 0.01$; * $p < 0.05$.
 802 **D**, AUC of Kiss1^{ARH} neurons from *Kiss1*^{Cre} and *Stim1*^{kko} mice from C. There was a significant difference (Unpaired
 803 *t*-test, $t_{(11)} = 2.430, *p = 0.0334$) between the two groups.

FIGURE 3



317 **Figure 3. Deletion of *Stim1* augments high-frequency optogenetic stimulation-induced slow EPSP**
318 **depolarization in *Kiss1*^{ARH} neurons.** **A**, representative gel image illustrating the mRNA expression of *Trpc5*
319 channel subunit in *Kiss1*^{ARH} neurons harvested from female mice. The expected size of PCR products for *Kiss1*
320 and *Trpc5* are indicated. *Trpc4* mRNA was not detected in *Kiss1*^{ARH} neurons. MM is the molecular marker; –RT
321 indicates a harvested *Kiss1* neuron reacted without RT; + indicates positive tissue control (with RT); – indicates
322 negative tissue control (without RT) using cDNA from mouse medial basal hypothalamic tissue; RT, reverse
323 transcriptase. **B**, quantitative single cell PCR (3 x 10 cell pools per animal, n = 3 animals) verified that *Trpc5* was
324 expressed in *Kiss1*^{ARH} neurons, whereas *Trpc4* mRNA was not detected (Unpaired t-test for the left, $t_{(4)} = 15.67$,

825 **** p < 0.0001). **C**, the I-V relationship for the Senk-induced inward current recorded in Kiss1^{ARH} neurons from
826 Kiss1^{Cre} mice using a Cs⁺ internal solution (n= 4) revealed a reversal of -10 mV and rectification. **D**, **E**, high-
827 frequency optogenetic stimulation (20 Hz, 10 s) generated slow EPSPs in a ChR2-expressing Kiss1^{ARH} neuron
828 from control Kiss1 mice (**D**) and in a ChR2-expressing Kiss1^{ARH} neuron from *Stim1*^{kk0} mice (**E**). The lower trace
829 shows the slow EPSP after low-pass filtering from D and E (arrow), respectively. **F**, summary of the effects of
830 *Stim1* deletion on the slow EPSP amplitude. Bar graphs represent the mean ± SEM (Unpaired t-test, $t_{(39)} =$
831 2.802, **p = 0.0079).

322 FIGURE 4

332

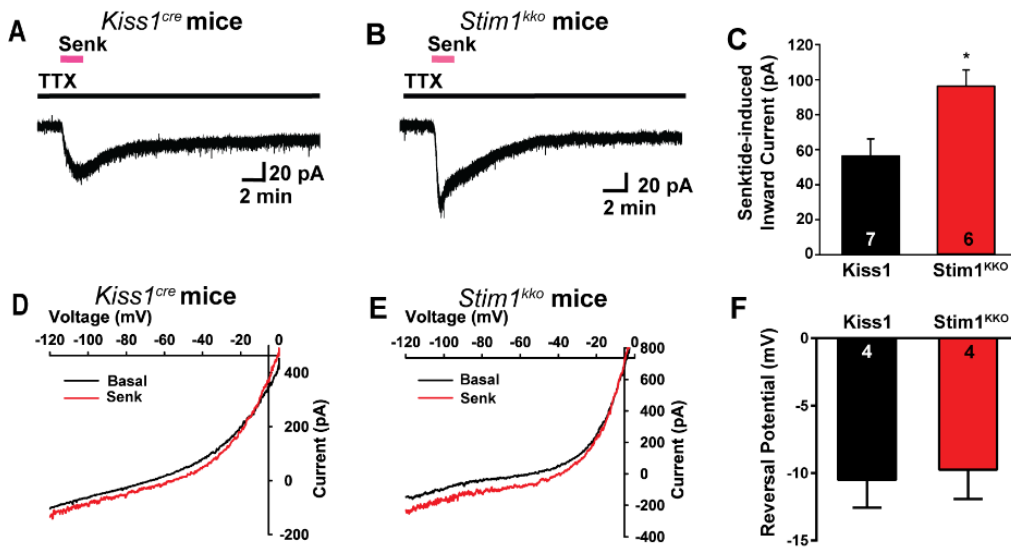


Figure 4. **Deletion of *Stim1* augments senktide-induced depolarization in Kiss1^{ARH} neurons.** **A** and **B**, rapid bath application of senktide (1 μ M) induced an inward current in the presence of fast sodium channel blockade (TTX, 1 μ M) in Kiss1^{ARH} neurons from *Kiss1*^{Cre} and *Stim1*^{kk0} mice. $V_{hold} = -60$ mV. **C**, summary of the effects of senktide in Kiss1^{ARH} neurons from *Kiss1*^{Cre} and *Stim1*^{kk0} mice (Unpaired t-test, $t_{(11)} = 2.929$, *p = 0.0137). Data points represent the mean ± SEM. Cell numbers are indicated. **D** and **E**, the I-V relationship before and during the peak response of senktide (Senk) in Kiss1^{ARH} neurons from *Kiss1*^{Cre} (**D**) and *Stim1*^{kk0} (**E**) mice indicated that the reversal potential of the nonselective cation current was ~ -10 mV. **F**, summary of the reversal potentials of the senktide-induced cation current recorded in Kiss1^{ARH} neurons from *Kiss1*^{Cre} and *Stim1*^{kk0} mice. Bar graphs represent the mean ± SEM (unpaired two-tailed t test, $t_{(6)} = 0.2503$, p = 0.8107).

352
353 **FIGURE 5**

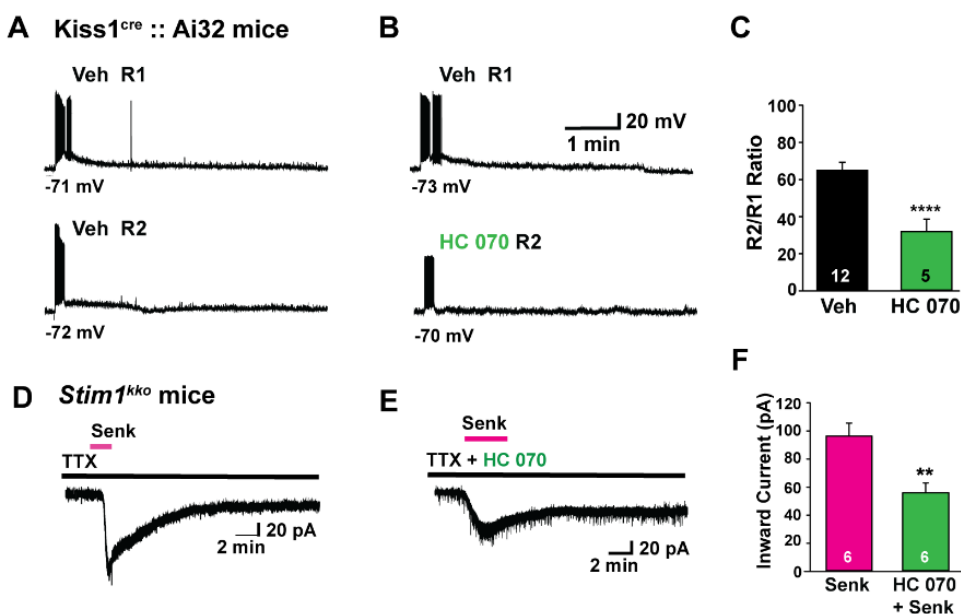
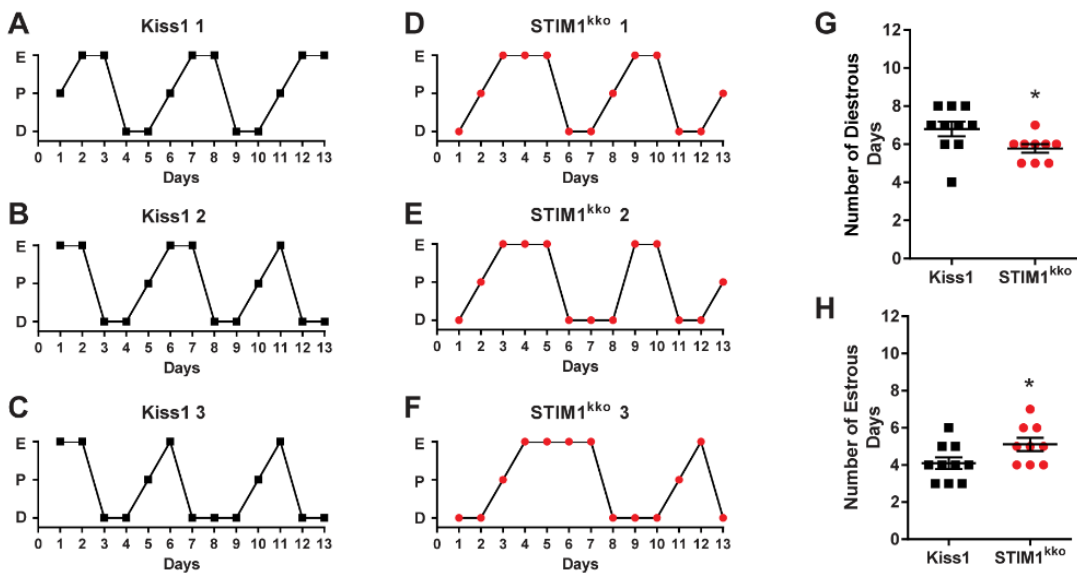


Figure 5. Stim1 deletion augments senktide-induced Kiss1^{ARH} neuronal excitability through TRPC channel activation. **A-C**, high frequency photo-stimulation – induced slow EPSP in Kiss1^{ARH} neurons from Kiss1^{Cre}::Ai32 mice is antagonized by TRPC5 channel blocker. **A–B**, representative traces of high-frequency optogenetic stimulation-induced slow EPSPs in the absence (A) or presence (B) of TRPC4/5 channel blocker HC 070 (100 nM). **C**, summary of the effects of HC 070 on the slow EPSP (Un-paired t-test, $t_{(15)} = 4.122$, $****p = 0.0009$). **D–F**, Stim1 deletion augments senktide-induced inward current, which is antagonized by the TRPC5 channel blocker. **D–E**, representative traces of senktide (1 μ M)-induced inward current in *Stim1*^{cko} neurons perfused with TTX (1 μ M) in the absence (D) or presence (E) of TRPC4/5 blocker HC 070 (100 nM). **F**, summary of the effects of HC 070 on the senktide-induced inward current (Un-paired t-test, $t_{(10)} = 3.457$, $**p = 0.0062$). Data points represent the mean \pm SEM. Cell numbers are indicated.

379
380 **FIGURE 6**
381



391 **Figure 6. *Stim1*^{ko} mice exhibit more estrous days.** A-F, representative estrous cycle data from three
392 representative control *Kiss1*^{Cre} and three *Stim1*^{ko} mice over a thirteen-day period. Vaginal lavage was done
393 daily at 0930 h, and cell cytology was observed and recorded as Diestrus (D), Proestrus (P) or Estrus (E).
394 Summary data for the number of Diestrous days (G) and Estrous days (H) during the 13 day period was
395 compared between *Kiss1*^{Cre} (n = 10) and *Stim1*^{ko} mice (n = 9) (unpaired, two-tailed t test for G, $t_{(17)} = 2.215$, *p
396 = 0.0407; unpaired two-tailed t-test for H, $t_{(17)} = 2.151$, *p = 0.0461).

397
398 **FIGURE 7**
399
400

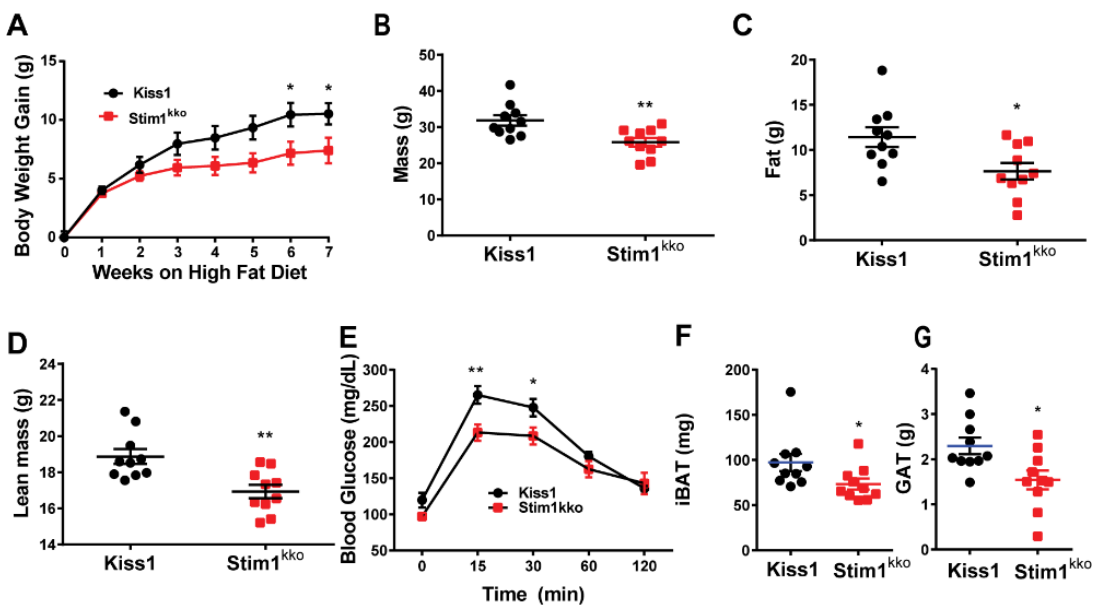


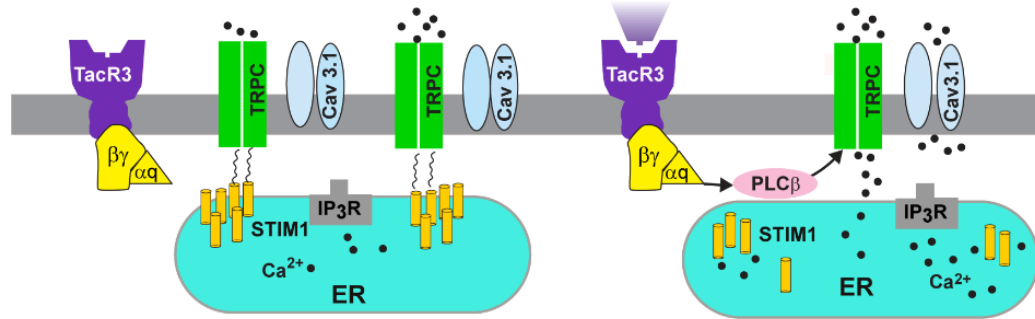
Figure 7. Ablation of *Stim1* in *Kiss1* neurons attenuates body mass, fat, and lean in mice on a high fat diet. *Stim1*^{kk0} and *Kiss1*^{Cre} littermate control females were ovariectomized and fed a high fat diet (HFD; 45% kcal from fat) for seven weeks. **A**, body-weight gain measured once a week for seven weeks. The high fat diet caused significant weight gain in both groups relative to their baseline with the *Kiss1*^{Cre} females gaining significantly more weight by 6 weeks [two-way ANOVA: main effect of treatment ($F_{(1, 18)} = 3.839$, $p = 0.0657$), main effect of time ($F_{(7, 126)} = 98.07$, $p < 0.0001$) and interaction ($F_{(7, 126)} = 4.645$, $p = 0.0001$); *Kiss1* control, $n = 10$, *Stim1*^{kk0}, $n = 10$; *post hoc* Bonferroni test, $*p < 0.05$]. **B-D**, mass (B), total body fat (C) and lean mass (D) measured by an EchoMRI Whole Body Composition Analyzer. Lean mass did not include bone and fluids within organs. The difference in mass (B), body fat (C) and lean mass (D) between the groups was significantly different by 6 weeks on high fat diet (unpaired, two-tailed t-test for B, $t_{(18)} = 3.222$, $**p = 0.0047$; unpaired two-tailed t test for C, $t_{(18)} = 2.662$, $*p = 0.0159$; unpaired, two-tailed t test for D, $t_{(18)} = 3.489$, $*p = 0.0026$). **E**, six weeks after high fat diet, there was a significant difference in GTTs between the two groups (two-way ANOVA: main effect of treatment ($F_{(1, 9)} = 6.282$, $p = 0.0335$), main effect of time ($F_{(4, 36)} = 88.01$, $p < 0.0001$) and interaction ($F_{(4, 36)} = 3.527$, $p = 0.0158$); *Kiss1*^{Cre}, $n = 6$, *Stim1*^{kk0}, $n = 5$; *post hoc* Bonferroni test, $**p < 0.01$, $*p < 0.05$). **F** and **G**, both interscapular brown adipose tissue (iBAT) and perigonadal adipose tissue (GAT) mass of *Stim1*^{kk0} were lighter

923 than that of *Kiss1^{Cre}* mice on a fat diet after eight weeks (unpaired, two-tailed t test for iBAT, $t_{(18)} = 2.127$, *p =
924 0.0475; unpaired two-tailed t-test for GAT, $t_{(18)} = 2.711$, *p = 0.0143).

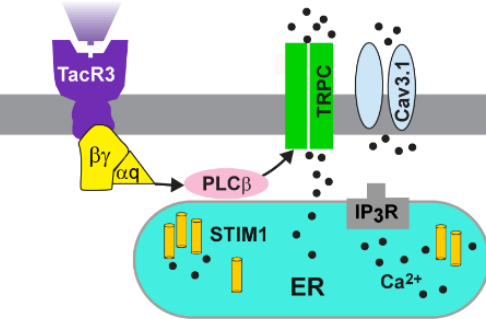
925

926 **FIGURE 8**

927 **A. Store Operated**



928 **B. Receptor Operated**



933

934 **Figure 8. A cellular model of STIM1 affecting NKB activation of TRPC5 channels in Kiss1^{ARH} neurons. A,**
935 Store-operated calcium entry (SOCE) is a conserved mechanism by which the depletion of the endoplasmic
936 reticulum (ER) is conveyed to calcium-permeable channels at the plasma membrane (PM), triggering calcium
937 influx from the extracellular space and into the cell cytosol. A physiological mechanism responsible for the
938 activation of SOCE results from the stimulation of G-protein coupled receptors associated with the inositol-
939 triphosphate (IP3) and phospholipase C cascade, resulting in the release of calcium from ER, via the IP3 receptor
940 (IP3R). Under physiological stress and in the absence of E₂, stromal interaction molecule 1 (STIM1) interacts
941 with TRPC5 channels thereby engaging these Ca²⁺ channels as store-operated channels, which are activated
942 with endoplasmic reticulum (ER) depletion of Ca²⁺. **B**, however, under physiological conditions in reproductively
943 active females, in which E₂ down-regulates the expression of STIM1, TRPC 5 channels are converted to
944 receptor-operated channels in Kiss1^{ARH} neurons. Neurokinin B (NKB) binds to its receptor (TacR3) to activate
945 G_{aq} – PLC_β signaling cascade to facilitate TRPC 5 channel opening, generating a robust inward Na⁺/Ca²⁺
946 current to depolarize Kiss1^{ARH} neurons, activating T-type calcium (Cav3.1) channels to greatly increase Kiss1^{ARH}
947 neuronal excitability.

950 **Table 1. Primer Table**

952	Gene Name	Accession	Primer	Product	Annealing	<u>Efficiency</u>		
953	<u>(encodes for)</u>	Number	<u>Location (nt)</u>	<u>Length (bp)</u>	<u>Temp (°C)</u>	Slope	r^2	%
954	<i>Kiss1</i> (Kiss1) ^{a,b}	NM_178260	64-80 (exon 1) 167-183 (exon 2)	120	57 ^a , 60 ^b	-3.410	0.989	97
955	<i>Stim1</i> (STIM1) ^a	NM_009287	797-816 (exon 2) 981-1000 (exon 3)	204	59			
956	<i>Stim1</i> (STIM1) ^b	NM_009287	821-839 (exon 2) 937-955 (exon 3)	135	60	-3.311	0.977	100
957	<i>Stim2</i> (STIM2) ^a	NM_001363348	620-638 (exon 2) 773-791 (exon 4)	172	59			
958	<i>Stim2</i> (STIM2) ^b	NM_001363348	1784-1803 (exon 11) 1895-1914 (exon 12)	131	60	-3.439	0.993	95
959	<i>Gapdh</i> (GAPDH) ^b	NM_008084	689-706 (exon 4) 764-781 (exon 5)	93	60	-3.352	0.998	99
960	<i>Trpc4</i> (TRPC4) ^{a,b}	NM_016984	1888-1907 (exon 6) 1984-2003 (exon 7)	116	60	-3.318	0.940	100
961	<i>Trpc5</i> (TRPC5) ^a	NM_009428	2206-2227 (exon 6) 2315-2336 (exon 7)	131	63			
962	<i>Trpc5</i> (TRPC5) ^b	NM_009428	734-753 (exon 2) 832-851 (exon 3)	118	60	-3.161	0.953	100
963								
964								
965								
966								
967								
968								
969								
970								
971								
972								
973	^a primers for scRT-PCR.							
974	^b primers for qPCR.							
975								
976								
977	Figure 2-video supplement 1. Neurokinin B receptor agonist senktide induces $[Ca^{2+}]_i$ increase in							
978	Kiss1^{ARH} neurons expressing GCaMP6s. Imaging of transient Ca^{2+} changes in an arcuate slice using spinning							
979	disk confocal microscopy. Fluorescence intensity was measured over 20 minutes, before and after application							

980 of senktide (1 μ M). The period represented is 20 minutes.

981

982 **Figure 3-video supplement 1. High frequency photo-stimulation induces a slow excitatory postsynaptic**
983 **potential (slow EPSP).** Slow EPSP was induced by a 10-s 20 Hz photostimulation (light intensity 0.9 mW and
984 pulse duration, 10 ms) in a ChR2-expressing Kiss1^{ARH} neuron in a slice from a *Kiss1*^{Cre}::*Ai32* mouse. The period
985 represented is 1 minute, 34 seconds.